

Numerical solution of the boundary value problem of elliptic equation by Levi function scheme

Jinchao Pan[†] Jijun Liu^{†‡*}

[†]School of Mathematics/Shing-Tung Yau Center of Southeast University
Southeast University

Nanjing, 210096, P.R.China

^{†‡}Nanjing Center for Applied Mathematics

Nanjing, 211135, P.R.China

May 28, 2024

Abstract

For boundary value problem of an elliptic equation with variable coefficients describing the physical field distribution in inhomogeneous media, the Levi function can represent the solution in terms of volume and surface potentials, with the drawback that the volume potential involving in the solution expression requires heavy computational costs as well as the solvability of the integral equations with respect to the density pair. We introduce an modified integral expression for the solution to an elliptic equation in divergence form under the Levi function framework. The well-posedness of the linear integral system with respect to the density functions to be determined is rigorously proved. Based on the singularity decomposition for the Levi function, we propose two schemes to deal with the volume integrals so that the density functions can be solved efficiently. One method is an adaptive discretization scheme (ADS) for computing the integrals with continuous integrands, leading to the uniform accuracy of the integrals in the whole domain, and consequently the efficient computations for the density functions. The other method is the dual reciprocity method (DRM) which is a meshless approach converting the volume integrals into boundary integrals equivalently by expressing the volume density as the combination of the radial basis functions determined by the interior grids. The proposed schemes are justified numerically to be of satisfactory computation costs. Numerical examples in 2-dimensional and 3-dimensional cases are presented to show the validity of the proposed schemes.

Keywords: Levi function, integral equations, solvability, adaptive scheme, numerics.

AMS Subject Classifications: 35L05, 35L10, 35R09

*Corresponding author: Prof. Dr. J.J.Liu, email: jjliu@seu.edu.cn

1 Introduction

For a bounded smooth domain $\Omega \subset \mathbb{R}^d$ with $d = 2, 3$, consider the system

$$\begin{cases} -\nabla \cdot (\sigma(x)\nabla u(x)) = F(x), & x \in \Omega, \\ u(x) = f(x), & x \in \partial\Omega \end{cases} \quad (1.1)$$

with $0 < \sigma_0 < \sigma(x) \in C(\overline{\Omega})$. It is well-known that there exists a unique solution $u \in H^1(\Omega)$ for given $F \in L^2(\Omega)$ and $f \in H^{1/2}(\partial\Omega)$, see [1]. The above boundary value problem is an mathematical model describing the distribution of electrical potential $u(x)$ with $\sigma(x)$ being the conductivity in conductive media $\Omega \subset \mathbb{R}^d$.

For the boundary value problem (1.1), it is well-known that the solution can be solved numerically by finite element method (FEM) for the domain Ω of general shape. Based on the variational form of (1.1), the solution u is obtained in the whole domain from its base function expansions constructing in terms of the mesh discretizations of the domain Ω . However, there exists another way to solve the solution u for the elliptic equation with constant coefficients, namely, the boundary elements method (BEM), which represents the solution in terms of the surface potential with some density function to be determined. Once the density function in the surface layer potential is determined from the boundary condition, the solution in every point of Ω is obtained by computing the surface integral defined in $\partial\Omega$. Such techniques have been studied for solving PDEs in different forms such as the Helmholtz equation, the Lamé system as well as the biharmoni equations, see [2]. The other applications of BEM are in the areas of inverse and ill-posed problems, where the adjoint operators are relatively easy to be derived due to the integral representations of the solution, when we find the regularizing solutions by minimizing the corresponding cost functional iteratively, see [3, 4, 5].

However, in the cases of the PDEs with variable coefficients governing the physical field in inhomogeneous media, the BEM scheme does not work anymore for finding its solution, since the fundamental solution to the differential operator with variable coefficients, although exists, cannot be represented explicitly. In these cases, it is also well-known that, the Levi function pair $(P(x, y), R(x, y))$ for elliptic operator $A(x, \partial)$ with variable coefficients defined by

$$A(x, \partial)P(x, y) = \delta(x - y) + R(x, y),$$

which is considered as the generalization of the fundamental solution, plays an important rule in theoretical studies for PDEs [6, 7].

Although such a generalized expression scheme has been studied thoroughly, the numerical realizations seem not to be implemented efficiently, due to the reason that the solvability of the corresponding integral system with respect to the density functions heavily depends on the potentials, e.g., the single-layer potential or double-layer one, as well as the form of boundary conditions. In [8], the system (1.1) with $F(x) = 0$ is solved numerically based on the solution representation

$$u(x) := \int_{\Omega} \mu(y)P(x, y)dy + \int_{\partial\Omega} \psi(y)P(x, y)ds(y) \quad (1.2)$$

for Levi function $P(x, y)$. The discretization scheme for solving the corresponding integral system is established there, the numerical examples show the potential efficiency of this scheme for (1.1), see also [9]. However, due to the single-layer representation $\int_{\partial\Omega} \psi(y)P(x, y)ds(y)$ in

(1.2), the derived boundary integral equation on $\partial\Omega$ from the Dirichlet boundary condition in (1.1) is of the first kind with respect to the density ψ . Consequently, the solvability of the corresponding integral system with respect to the density pair (μ, ψ) cannot be ensured, which means the Levi function scheme (1.2) for solving (1.1) is still questionable.

On the other hand, the domain integral in (1.2) involving the density μ to be determined is the novel and necessary term of Levi function scheme for solving PDE with variable coefficients. Therefore we need to evaluate the first term in (1.2) in an efficient way for obtaining the solution u with satisfactory accuracy. An efficient way to the computation of this domain integral, as proposed in [8] for $\Omega \subset \mathbb{R}^2$, is to establish the domain transform Π to Ω in terms of known coordinates transform, where Π is a standard rectangle domain. Then the first term in (1.2) can be discretized in the new coordinate in Π . However, the coordinates transform, although enables us to compute the integral in a rectangle domain Π which is easy to be partitioned, may change the area of each elements in Ω non-uniformly due to the fact that the Jacobian determinant depends on the position of the elements. This new phenomenon requires some nonuniform partition in Π for computing the integral in Ω with a uniform accuracy, otherwise the density function μ in Ω will be of different accuracy and consequently contaminates the accuracy of u for (1.1) from the Levi function representation. Moreover, to compute the volume potential accurately, the domain Ω should be partitioned into elements with very small size, and consequently the evaluations of the unknown μ at the partition grids lead to the solution of a linear algebra equations of large size, which is of heavy computational cost. To overcome this difficulty, a possible way is to convert the domain integral in Ω into the boundary integral on $\partial\Omega$ by expanding the density function μ in terms of some specified base functions, such as the dual reciprocity method (DRM) [10] or the radial integration method (RIM) [11].

Based on the above motivations, we make novel contributions for numerically solving (1.1) under the Levi function framework from three aspects. Firstly, instead of the single layer boundary potential in (1.2) for the representation of the solution, we apply the double-layer potential, which is different from those in [7] and leads to a linear integral equation of the second kind for the density pair (μ, ψ) . Secondly, the solvability of this linear system is established rigorously in two different function spaces, which ensures the applicability of the Levi function scheme for (1.1). Finally, after the standard singularity decompositions dealing with the hyper-singularity of the integral term in the linear system coming from the double layer potential, we propose two discrete schemes for computing the volume potential efficiently, namely, the self-adaptive partition scheme (ADS) with explicit quantitative criterion for the non-uniform partition of Ω and the dual reciprocity method (DRM) leading to a domain discretization-free method. The proposed two schemes for solving the density function pair provide efficient numerical realizations of solving (1.2) in terms of the Levi function framework. Numerical experiments show that the proposed schemes can yield the solution u on arbitrary internal points with satisfactory accuracy compatible to well-known finite element methods (FEM).

In general, the treatments of the solution of elliptic equation with variable coefficients under the framework of integral equations, as pointed in [8], are realized in three main ways. The first scheme is to decompose the variable coefficient into a constant and a non-constant part, then the term with the variable coefficient is viewed as a source term, and the direct integral equation approach leads to a boundary-domain integral equation [12, 13, 14]. The second scheme is based on the Green's formula in combination with a Levi function [15, 16, 17]. The third way is what we consider here, namely, the indirect integral equation formulation using potential representation of the solution by Levi functions.

We organize the paper as follows. In section 2, we establish a boundary integral equation system for the density pair (μ, ψ) under the Levi function scheme for computing the solution to (1.1). This new system is different from the cases for the Laplace or the Helmholtz equations with constant coefficients which involve only the surface potentials. The solvability of the coupled system is rigorously proving in two different spaces. Then in section 3, we propose to solve the corresponding linear system with a self-adaptive scheme (ADS) with explicit quantitative criterion for dealing with the smooth integrands, while the singularities in the kernel functions are decomposed from the property of the Levi function, and then can be computed from the well-known quadrature rules. In section 4, the dual reciprocity method (DRM) which transforms the domain integrals into boundary integrals is applied to compute the volume potential without domain discretization. The choice of interior nodes for constructing the base functions are random and DRM can compute the weak singularity in volume potential explicitly by transforming the volume integrals into boundary integrals. In section 5, numerical experiments of our proposed schemes are implemented for 2-dimensional and 3-dimensional cases, showing the validity by comparing the numerics with finite element methods.

2 Integral representation of the solution

For differential operator $\mathcal{L}\diamond := -\nabla \cdot (\sigma \nabla \diamond)$ in \mathbb{R}^d , we call the function $P(x, y)$ with $x, y \in \mathbb{R}^d$ the Levi function, provided

$$\mathcal{L}_x P(x, y) = \delta(x - y) + R(x, y) \quad (2.1)$$

in the distribution sense, where δ is the standard Dirac function, and $R(x, y)$ is a function of weak singularity for $x = y$. Notice, the Levi function $P(x, y)$ and consequently the reminder $R(x, y)$ are not unique.

Introduce the fundamental solution

$$\Phi(x, y) := \begin{cases} \frac{1}{2\pi} \ln \frac{1}{|x-y|}, & d = 2 \\ \frac{1}{4\pi} \frac{1}{|x-y|}, & d = 3 \end{cases}$$

to the Laplacian operator, i.e., $-\Delta_x \Phi(x, y) = \delta(x - y)$. It is well known that one of the form of the Levi function pair for \mathcal{L} is

$$\begin{aligned} (P(x, y), R(x, y)) &= \frac{1}{\sigma(y)} (\Phi(x, y), -\nabla_x \Phi(x, y) \cdot \nabla \sigma(x)) \\ &= \begin{cases} \left(\frac{1}{\sigma(y)} \frac{1}{2\pi} \ln \frac{1}{|x-y|}, \frac{1}{\sigma(y)} \frac{(x-y) \cdot \nabla \sigma(x)}{2\pi |x-y|^2} \right), & d = 2 \\ \left(\frac{1}{\sigma(y)} \frac{1}{4\pi |x-y|}, \frac{1}{\sigma(y)} \frac{(x-y) \cdot \nabla \sigma(x)}{4\pi |x-y|^3} \right), & d = 3 \end{cases} \end{aligned} \quad (2.2)$$

for $x \neq y$. Note, $R(x, y)$ is of the weak singularity from $|R(x, y)| \leq C|x - y|^{-(d-1)}$.

The classical Levi function scheme represents the solution to (1.1) by (1.2), which can be considered as a combination of the volume potential in Ω and the single-layer potential in $\partial\Omega$. Then by inserting this representation into both the equation and the boundary condition in (1.1), a linear system with respect to the density pair $(\mu|_{\Omega}, \psi|_{\partial\Omega})$ is derived. However, the corresponding integral equation from the boundary condition is the first kind, and consequently,

the solvability of the derived integral system, i.e., the reasonability of the standard Levi function scheme, cannot be ensured theoretically, although this scheme has been realized efficiently. To overcome such a shortcoming, we propose to modify the representation (1.2) as

$$u(x) = \int_{\Omega_{\epsilon_0}} \mu(y)P(x, y)dy + \int_{\partial\Omega} \frac{\psi(y)}{\sigma(y)} \partial_{\nu(y)}\Phi(x, y)ds(y), \quad x \in \Omega \quad (2.3)$$

for some density functions $\mu \in C(\overline{\Omega_{\epsilon_0}})$ and $\psi \in C(\partial\Omega)$, where $\Omega_{\epsilon_0} \subset\subset \Omega$ is arbitrary specified domain. Notice, the volume potential (2.3) is defined in the interior domain Ω_{ϵ_0} instead of the whole domain Ω , which is crucial for us to avoid the hyper-singularity of double-layer potential in (2.3) in the PDE in Ω . By the $C^1(\mathbb{R}^d)$ regularity of volume potential (Theorem 8.1, [5]) and the jump relation of the double potential potential as well as the continuity of the single potential (Theorem 2.13, Theorem 2.12, [18]), if $u(x)$ represented by (2.3) solves (1.1), $(\mu, \psi) \in C(\overline{\Omega_{\epsilon_0}}) \times C(\partial\Omega)$ must solve

$$\begin{cases} \mu(x) + \int_{\Omega_{\epsilon_0}} \mu(y)R(x, y)dy + \int_{\partial\Omega} \frac{\psi(y)}{\sigma(y)} \partial_{\nu(y)}(\sigma(y)R(x, y))ds(y) = F(x), & x \in \Omega_{\epsilon_0} \\ \int_{\Omega_{\epsilon_0}} \mu(y)P(x, y)dy + \int_{\partial\Omega} \frac{\psi(y)}{\sigma(y)} \partial_{\nu(y)}\Phi(x, y)ds(y) - \frac{1}{2} \frac{\psi(x)}{\sigma(x)} = f(x), & x \in \partial\Omega. \end{cases} \quad (2.4)$$

In case of $(\sigma(x), F(x)) \equiv (1, 0)$, it follows from the first equation that $\mu(x) \equiv 0$ and the second equation in (2.4) is just the boundary integral equation of the second kind with respect to the density function $\psi(x)$ for solving the interior Dirichlet problem for the Laplace equation in Ω , noticing that Ω_{ϵ_0} is the arbitrary domain in Ω .

In the following we only consider 2-dimensional space. However, all the arguments work for the case $d = 3$ with obvious modifications on the fundamental solution.

Define $\tilde{\mu}(x) := \frac{\mu(x)}{\sigma(x)}$ for $x \in \overline{\Omega_{\epsilon_0}}$ and $\tilde{\psi}(x) := \frac{\psi(x)}{\sigma(x)}$ for $x \in \partial\Omega$, and the operators

$$\begin{aligned} \mathbb{K}_{11}^{\Omega_{\epsilon_0} \rightarrow \overline{\Omega_{\epsilon_0}}}[\tilde{\mu}](x) &:= \int_{\Omega_{\epsilon_0}} \nabla_x \Phi(x, y) \cdot \nabla \ln \sigma(x) \tilde{\mu}(y) dy, & x \in \overline{\Omega_{\epsilon_0}}, \\ \mathbb{K}_{12}^{\partial\Omega \rightarrow \overline{\Omega_{\epsilon_0}}}[\tilde{\psi}](x) &:= - \int_{\partial\Omega} \frac{\partial}{\partial \nu(y)} (\nabla_x \Phi(x, y) \cdot \nabla \ln \sigma(x)) \tilde{\psi}(y) ds(y), & x \in \overline{\Omega_{\epsilon_0}}, \\ \mathbb{K}_{21}^{\Omega_{\epsilon_0} \rightarrow \partial\Omega}[\tilde{\mu}](x) &:= -2 \int_{\Omega_{\epsilon_0}} \Phi(x, y) \tilde{\mu}(y) dy, & x \in \partial\Omega, \\ \mathbb{K}_{22}^{\partial\Omega \rightarrow \partial\Omega}[\tilde{\psi}](x) &:= 2 \int_{\partial\Omega} \frac{\partial \Phi(x, y)}{\partial \nu(y)} \tilde{\psi}(y) ds(y), & x \in \partial\Omega. \end{aligned}$$

Then we can rewrite (2.4) in the operator form

$$\begin{cases} (\mathbb{I} - \mathbb{K}_{11}^{\Omega_{\epsilon_0} \rightarrow \overline{\Omega_{\epsilon_0}}})[\tilde{\mu}](z) + \mathbb{K}_{12}^{\partial\Omega \rightarrow \overline{\Omega_{\epsilon_0}}}[\tilde{\psi}](z) = F(z)\sigma^{-1}(z), & z \in \Omega_{\epsilon_0} \\ \mathbb{K}_{21}^{\Omega_{\epsilon_0} \rightarrow \partial\Omega}[\tilde{\mu}](x) + (\mathbb{I} - \mathbb{K}_{22}^{\partial\Omega \rightarrow \partial\Omega})[\tilde{\psi}](x) = -2f(x), & x \in \partial\Omega. \end{cases} \quad (2.5)$$

We firstly establish the solvability of (2.5) for the density function pair in continuous function space for known (σ, F, f) by the following result.

Theorem 2.1. *Assume that the specified conductivity in (1.1) meets $0 < \sigma_0 \leq \sigma \in C^1(\overline{\Omega})$ and*

$$0 \leq \|\nabla \ln \sigma\|_{C(\overline{\Omega})} \ll 1. \quad (2.6)$$

Then for any $(F, f) \in C(\overline{\Omega}) \times C(\partial\Omega)$, there exists a unique solution $(\tilde{\mu}, \tilde{\psi}) \in C(\overline{\Omega}_{\epsilon_0}) \times C(\partial\Omega)$ to (2.5), where $\Omega_{\epsilon_0} := \{x \in \Omega : \text{dist}(x, \partial\Omega) \geq \epsilon_0\}$ with any small $\epsilon_0 > 0$. Moreover, $u(x, t)$ defined by (2.3) meets the PDE in Ω_{ϵ_0} and the the boundary condition in $\partial\Omega$.

In case of $\nabla\sigma|_{\Omega} \equiv 0$ with $F = 0$, i.e., σ is a constant in Ω , we can solve the direct problem using single layer potential directly, i.e., we can specify $\mu(x) \equiv 0$ in (2.3).

Proof. We prove this result by using the Fredholm Alternative and the contractive mapping recursively.

We rewrite (2.5) equivalently in the vector form

$$(\mathbb{I} - \mathbb{K}_{\sigma}) \begin{bmatrix} \tilde{\mu} \\ \tilde{\psi} \end{bmatrix} \begin{pmatrix} z \\ x \end{pmatrix} = \begin{pmatrix} F(z)\sigma^{-1}(z) \\ -2f(x) \end{pmatrix}, \quad (z, x) \in \Omega_{\epsilon_0} \times \partial\Omega \quad (2.7)$$

with the matrix operator

$$\mathbb{K}_{\sigma} := \begin{pmatrix} \mathbb{K}_{11}^{\Omega_{\epsilon_0} \rightarrow \Omega_{\epsilon_0}} & -\mathbb{K}_{12}^{\partial\Omega \rightarrow \Omega_{\epsilon_0}} \\ -\mathbb{K}_{21}^{\Omega_{\epsilon_0} \rightarrow \partial\Omega} & \mathbb{K}_{22}^{\partial\Omega \rightarrow \partial\Omega} \end{pmatrix}.$$

By the expressions of four elements of the matrix \mathbb{K}_{σ} , \mathbb{K}_{σ} is compact from $C(\overline{\Omega}_{\epsilon_0}) \times C(\partial\Omega)$ to itself. Notice, both $\mathbb{K}_{21}^{\Omega_{\epsilon_0} \rightarrow \partial\Omega}$ and $\mathbb{K}_{12}^{\partial\Omega \rightarrow \Omega_{\epsilon_0}}$ are of continuous kernel due to $\overline{\Omega}_{\epsilon_0} \subset\subset \Omega$. Therefore, to prove Theorem 2.1, it is enough to prove the uniqueness of the solution to (2.7) by the Fredholm Alternative for the linear compact operator equation of the second kind.

The uniqueness of solution to (2.7) (equivalently to (2.5)) is established by several steps. Assume that $(\tilde{\mu}, \tilde{\psi}) \in C(\overline{\Omega}_{\epsilon_0}) \times C(\partial\Omega)$ meets

$$\begin{cases} (\mathbb{I} - \mathbb{K}_{11}^{\Omega_{\epsilon_0} \rightarrow \Omega_{\epsilon_0}})[\tilde{\mu}](z) + \mathbb{K}_{12}^{\partial\Omega \rightarrow \Omega_{\epsilon_0}}[\tilde{\psi}](z) = 0, & z \in \Omega_{\epsilon_0}, \\ \mathbb{K}_{21}^{\Omega_{\epsilon_0} \rightarrow \partial\Omega}[\tilde{\mu}](x) + (\mathbb{I} - \mathbb{K}_{22}^{\partial\Omega \rightarrow \partial\Omega})[\tilde{\psi}](x) = 0, & x \in \partial\Omega. \end{cases} \quad (2.8)$$

We need to prove $(\tilde{\mu}, \tilde{\psi}) = (0, 0)$.

Step 1: We prove that the equation

$$(\mathbb{I} - \mathbb{K}_{11}^{\Omega_{\epsilon_0} \rightarrow \Omega_{\epsilon_0}})[\tilde{\mu}](z) = g(z), \quad z \in \Omega_{\epsilon_0}$$

is uniquely solvable for any $g \in C(\Omega_{\epsilon_0})$.

Since $\mathbb{K}_{11}^{\Omega_{\epsilon_0} \rightarrow \Omega_{\epsilon_0}}$ is compact from $C(\overline{\Omega}_{\epsilon_0})$ to itself, it is enough to prove

$$(\mathbb{I} - \mathbb{K}_{11}^{\Omega_{\epsilon_0} \rightarrow \Omega_{\epsilon_0}})[\tilde{\mu}](z) = 0$$

has only the trivial solution by the Fredholm Alternative. To this end, let us prove that the map $\mathbb{K}_{11}^{\Omega_{\epsilon_0} \rightarrow \Omega_{\epsilon_0}}$ is contractive. By the expression of $\mathbb{K}_{11}^{\Omega_{\epsilon_0} \rightarrow \Omega_{\epsilon_0}}$, we know

$$\|\mathbb{K}_{11}^{\Omega_{\epsilon_0} \rightarrow \Omega_{\epsilon_0}}[\tilde{\mu}]\|_{C(\overline{\Omega}_{\epsilon_0})} \leq \frac{\|\nabla \ln \sigma\|_{C(\overline{\Omega})}}{2\pi} \left\| \int_{\Omega_{\epsilon_0}} |\nabla_y \ln |y - \cdot| | dy \right\|_{C(\overline{\Omega}_{\epsilon_0})} \|\tilde{\mu}\|_{C(\overline{\Omega}_{\epsilon_0})}. \quad (2.9)$$

Since Ω is bounded and $\Omega_{\epsilon_0} \subset\subset \Omega$, $\mathbb{K}_{11}^{\Omega_{\epsilon_0} \rightarrow \Omega_{\epsilon_0}}$ is contractive from (2.9) and (2.6).

Step 2: Derive a linear equation for $\tilde{\psi}$ in fixed point form by (2.8).

By **Step 1**, we can solve $\tilde{\mu}$ explicitly from the first equation of (2.8), that is,

$$\tilde{\mu}(y) = -(\mathbb{I} - \mathbb{K}_{11}^{\Omega_{\epsilon_0} \rightarrow \Omega_{\epsilon_0}})^{-1} \mathbb{K}_{12}^{\partial\Omega \rightarrow \Omega_{\epsilon_0}} [\tilde{\psi}](y), \quad y \in \Omega_{\epsilon_0}. \quad (2.10)$$

Inserting this representation into the second equation of (2.8), we have

$$(\mathbb{I} - \mathbb{K}_{22}^{\partial\Omega \rightarrow \partial\Omega}) [\tilde{\psi}](x) - \mathbb{K}_{21}^{\Omega_{\epsilon_0} \rightarrow \partial\Omega} (\mathbb{I} - \mathbb{K}_{11}^{\Omega_{\epsilon_0} \rightarrow \Omega_{\epsilon_0}})^{-1} \mathbb{K}_{12}^{\partial\Omega \rightarrow \Omega_{\epsilon_0}} [\tilde{\psi}](x) = 0, \quad x \in \partial\Omega. \quad (2.11)$$

Since $\mathbb{K}_{22}^{\partial\Omega \rightarrow \partial\Omega}$ is double-layer potential with respect to the continuous density functions $\tilde{\psi}(y)$, it is compact from $C(\partial\Omega)$ to itself (Theorem 2.30 and Theorem 2.31 in [18]). So (2.11) leads to

$$(\mathbb{I} - \mathbb{K}_{22}^{\partial\Omega \rightarrow \partial\Omega}) [\tilde{\psi}](x) - \mathbb{K}^{\partial\Omega \rightarrow \partial\Omega} [\tilde{\psi}](x) = 0, \quad x \in \partial\Omega, \quad (2.12)$$

with the operator

$$\mathbb{K}^{\partial\Omega \rightarrow \partial\Omega} [\tilde{\psi}](x) := \mathbb{K}_{21}^{\Omega_{\epsilon_0} \rightarrow \partial\Omega} (\mathbb{I} - \mathbb{K}_{11}^{\Omega_{\epsilon_0} \rightarrow \Omega_{\epsilon_0}})^{-1} \mathbb{K}_{12}^{\partial\Omega \rightarrow \Omega_{\epsilon_0}} [\tilde{\psi}](x), \quad x \in \partial\Omega.$$

Notice that the operator $\mathbb{K}_{22}^{\partial\Omega \rightarrow \partial\Omega}$ is the double-layer potential for the Laplace operator, the unique solvability of the interior Dirichlet problem for the Laplace equation together with the double-layer potential representation of the solution ensures $\mathbb{I} - \mathbb{K}_{22}^{\partial\Omega \rightarrow \partial\Omega}$ is invertible from $C(\partial\Omega)$ to itself. So the equation (2.12) has the fixed-point form

$$\tilde{\psi}(x) - (\mathbb{I} - \mathbb{K}_{22}^{\partial\Omega \rightarrow \partial\Omega})^{-1} \mathbb{K}^{\partial\Omega \rightarrow \partial\Omega} [\tilde{\psi}](x) = 0, \quad x \in \partial\Omega. \quad (2.13)$$

Step 3: We prove that the equation (2.8) has only the trivial solution.

It is obvious that

$$\left\| \mathbb{K}_{21}^{\Omega_{\epsilon_0} \rightarrow \partial\Omega} \right\|_{C(\bar{\Omega}_{\epsilon_0}) \rightarrow C(\partial\Omega)} \leq C \quad (2.14)$$

due to $\Omega_{\epsilon_0} \subset\subset \Omega$. As for the operator $\mathbb{K}_{12}^{\partial\Omega \rightarrow \Omega_{\epsilon_0}}$, the straightforward computations yield

$$\mathbb{K}_{12}^{\partial\Omega \rightarrow \Omega_{\epsilon_0}} [\tilde{\psi}](x) \equiv \nabla_x \left(\mathbb{K}_{12,0}^{\partial\Omega \rightarrow \Omega_{\epsilon_0}} [\tilde{\psi}](x) \right) \cdot \nabla \ln \sigma(x), \quad (2.15)$$

where

$$\mathbb{K}_{12,0}^{\partial\Omega \rightarrow \Omega_{\epsilon_0}} [\tilde{\psi}](x) := - \int_{\partial\Omega} \frac{\partial\Phi(x,y)}{\partial\nu(y)} \tilde{\psi}(y) ds(y), \quad x \in \Omega_{\epsilon_0},$$

which is the double-layer potential with density function $\tilde{\psi}$. Since both kernels are smooth, we have from (2.15) that

$$\begin{aligned} \left\| \mathbb{K}_{12}^{\partial\Omega \rightarrow \Omega_{\epsilon_0}} [\tilde{\psi}] \right\|_{C(\Omega_{\epsilon_0})} &= \left\| \nabla_x (\mathbb{K}_{12,0}^{\partial\Omega \rightarrow \Omega_{\epsilon_0}} [\tilde{\psi}]) \cdot \nabla \ln \sigma \right\|_{C(\bar{\Omega}_{\epsilon_0})} \\ &\leq C_{\epsilon_0} \|\tilde{\psi}\|_{C(\partial\Omega)} \|\nabla \ln \sigma\|_{C(\bar{\Omega}_{\epsilon_0})} \leq C_{\epsilon_0} \|\nabla \ln \sigma\|_{C(\bar{\Omega})} \|\tilde{\psi}\|_{C(\partial\Omega)}, \end{aligned}$$

which yields

$$\left\| \mathbb{K}_{12}^{\partial\Omega \rightarrow \Omega_{\epsilon_0}} \right\|_{C(\partial\Omega) \rightarrow C(\bar{\Omega}_{\epsilon_0})} \leq C_{\epsilon_0} \|\nabla \ln \sigma\|_{C(\bar{\Omega})}. \quad (2.16)$$

Since both $(\mathbb{I} - \mathbb{K}_{22}^{\partial\Omega \rightarrow \partial\Omega})^{-1}$ and $(\mathbb{I} - \mathbb{K}_{11}^{\Omega_{\epsilon_0} \rightarrow \Omega_{\epsilon_0}})^{-1}$ are bounded, $(\mathbb{I} - \mathbb{K}_{22}^{\partial\Omega \rightarrow \partial\Omega})^{-1} \mathbb{K}^{\partial\Omega \rightarrow \partial\Omega}$ is contractive under (2.9), by combining (2.13), (2.14) and (2.16) together. So we have $\tilde{\psi}(x) = 0$ from (2.13). Finally we obtain $\tilde{\mu}(x) = 0$ from (2.10).

The assertion that $u(x)$ meets PDE in Ω_{ϵ_0} comes from (2.4). The proof is complete. \square

Since Ω_{ϵ_0} can approximate Ω up to any accuracy by taking $\epsilon_0 > 0$ small enough, we finally get the representation of $u(x)$ in Ω .

Remark 2.2. *The importance of this result is that we construct an implementable Levi-function-based scheme for solving the solution $u(x)$ to (1.1) in any interior domain Ω_{ϵ_0} in terms of (2.3), by proving the solvability of the density pair $(\tilde{\mu}|_{\Omega_{\epsilon_0}}, \tilde{\psi}|_{\partial\Omega})$ from (2.5) rigorously. The restriction that u satisfies the PDE in Ω_{ϵ_0} , namely, the requirement that, the first equation of (2.5) hold only in Ω_{ϵ_0} instead of Ω , enables us to keep the compact property of the operator $\mathbb{K}_{12}^{\partial\Omega \rightarrow \Omega_{\epsilon_0}}$ from its C^1 -smoothness for $\psi \in C(\partial\Omega)$, while the second equation of (2.5) is a linear integral equation of the second kind. However, for general $\sigma \in C^1(\bar{\Omega})$, if we consider the operators $\mathbb{K}_{12}^{\partial\Omega \rightarrow \Omega}$, which is not compact for $\tilde{\psi} \in C(\partial\Omega)$, the higher regularity $\tilde{\psi} \in C^{1,\alpha}(\partial\Omega)$ with $\alpha \in (0, 1)$ should be imposed (Theorem 2.23, [18]).*

Theorem 2.1 establishes the solvability of (2.7) in continuous function space for σ with slight restrictions, which ensures the reasonability of the Levi function representation (2.3) for solving (1.1), by firstly restricting the solution representation in Ω_{ϵ_0} and then taking $\epsilon_0 > 0$ arbitrary small. However, it is well-known that (1.1) is solvable for all $0 < \sigma \in L^\infty(\Omega)$. So, an interesting problem is to relax the restriction on σ in Theorem 2.1, removing the *a-priori* smallness assumption on $\|\nabla \ln \sigma\|_{C(\bar{\Omega})}$. We state this result in L^2 space as follows.

For any $(F, f) \in L^2(\Omega) \times L^2(\partial\Omega)$, define the density pair $(\mu, \psi) \in L^2(\Omega) \times L^2(\partial\Omega)$ from the solution to

$$\begin{cases} \mu(x) + \int_{\Omega} \mu(y)R(x, y)dy + \int_{\partial\Omega} \frac{\psi(y)}{\sigma(y)} \partial_{\nu(y)} \sigma(y)R(x, y)ds(y) = F(x), & x \in \Omega \\ \int_{\Omega} \mu(y)P(x, y)dy + \int_{\partial\Omega} \psi(y) \partial_{\nu(y)} P(x, y)ds(y) - \frac{1}{2} \frac{\psi(x)}{\sigma(x)} = f(x), & x \in \partial\Omega. \end{cases} \quad (2.17)$$

Theorem 2.3. *There exists a unique solution $(\mu, \psi) \in L^2(\Omega) \times L^2(\partial\Omega)$ to (2.17). Moreover, the function*

$$u(x) := \int_{\Omega} \mu(y)P(x, y)dy + \int_{\partial\Omega} \frac{\psi(y)}{\sigma(y)} \partial_{\nu(y)} \Phi(x, y)ds(y), \quad x \in \mathbb{R}^2 \quad (2.18)$$

solves the direct problem (1.1).

Proof. We firstly prove the uniqueness of the solution to (2.17). It is easy to verify from the jump relations of the surface potentials that $u \in H^2(\Omega)$ given by (2.18) with density pair (μ, ψ) satisfying (2.17) for $F = f = 0$ solves

$$\begin{cases} -\nabla \cdot (\sigma \nabla u) = 0, & x \in \Omega \\ u(x) = 0, & x \in \partial\Omega, \end{cases}$$

which yields

$$u(x) = \int_{\Omega} \Phi(x, y) \frac{\mu(y)}{\sigma(y)} dy + \int_{\partial\Omega} \frac{\partial \Phi(x, y)}{\partial \nu(y)} \frac{\psi(y)}{\sigma(y)} ds(y) \equiv 0 \quad (2.19)$$

for $x \in \Omega$. However, $u(x)$ representing by (2.18) also satisfies the exterior problem

$$\begin{cases} \Delta u = 0, & x \in \mathbb{R}^2 \setminus \bar{\Omega} \\ u(x) = 0, & x \in \partial\Omega \end{cases}$$

with zero asymptotic behavior as $|x| \rightarrow \infty$. Consequently we also have

$$u(x) = \int_{\Omega} \Phi(x, y) \frac{\mu(y)}{\sigma(y)} dy + \int_{\partial\Omega} \frac{\partial\Phi(x, y)}{\partial\nu(y)} \frac{\psi(y)}{\sigma(y)} ds(y) \equiv 0 \quad (2.20)$$

for $x \in \mathbb{R}^2 \setminus \bar{\Omega}$. Taking $x \rightarrow \partial\Omega$ from Ω and $\mathbb{R}^2 \setminus \bar{\Omega}$ in (2.19) and (2.20) respectively, the continuity of single layer potential and the volume potential on $\partial\Omega$ together with the jump relation of double layer potential on $\partial\Omega$ yields

$$\int_{\Omega} \Phi(x, y) \frac{\mu(y)}{\sigma(y)} dy + \int_{\partial\Omega} \frac{\partial\Phi(x, y)}{\partial\nu(y)} \frac{\psi(y)}{\sigma(y)} ds(y) \pm \frac{1}{2} \frac{\psi(x)}{\sigma(x)} \equiv 0, \quad x \in \partial\Omega,$$

which generate $\frac{\psi(x)}{\sigma(x)} \equiv 0$ in $\partial\Omega$ by subtracting these two identities. Then (2.17) for $F = f = 0$ leads to

$$(\mathbb{I} - \mathbb{K}_{11}^{\Omega \rightarrow \Omega}) \left[\frac{\mu}{\sigma} \right](x) = 0, \quad x \in \Omega \quad (2.21)$$

$$\mathbb{K}_{21}^{\Omega \rightarrow \partial\Omega} \left[\frac{\mu}{\sigma} \right](x) = 0, \quad x \in \partial\Omega, \quad (2.22)$$

where $(\mathbb{K}_{11}^{\Omega \rightarrow \Omega}, \mathbb{K}_{21}^{\Omega \rightarrow \partial\Omega})$ is $(\mathbb{K}_{11}^{\Omega_{\epsilon_0} \rightarrow \Omega_{\epsilon_0}}, \mathbb{K}_{21}^{\Omega_{\epsilon_0} \rightarrow \partial\Omega})$ with Ω_{ϵ_0} replaced by Ω .

Define $w(x) = \int_{\Omega} \Phi(x, y) \frac{\mu(y)}{\sigma(y)} dy$, $x \in \bar{\Omega}$ and noticing $-\Delta w = \frac{\mu(x)}{\sigma(x)}$ in Ω , then the above relations yield

$$-\frac{1}{\sigma(x)} \nabla \cdot (\sigma(x) \nabla w(x)) \equiv -\Delta w(x) - \nabla w(x) \cdot \nabla \ln \sigma(x) = 0, \quad x \in \Omega \quad (2.23)$$

$$w(x) = 0, \quad x \in \partial\Omega, \quad (2.24)$$

which leads to $w(x) = 0$ in Ω and then $\mu(x) = 0$ in Ω .

Noticing the fact that $\mathbb{K}_{11}^{\Omega \rightarrow \Omega}$ is also compact from $L^2(\Omega)$ to $L^2(\Omega)$ (Theorem 8.2 in [5]), (2.17) is a linear operator system of the second kind with compact operator \mathbb{K}_{σ} , so the Fredholm Alternative leads to the existence of the solution to (2.17) for any $(F, f) \in L^2(\Omega) \times L^2(\partial\Omega)$. The proof is complete. \square

For known $\sigma(x)$, we can firstly solve the density function $(\tilde{\mu}, \tilde{\psi})$ from the linear integral system (2.5) which is well-posed in terms of Theorem 2.1 and Theorem 2.3, and then determine the solution u to (1.1) using the representation (2.3). Since the operators in (2.5) are defined by integrals with singular kernels and also the domain integral, we need to establish the discrete version (2.5), dealing with the singularities and constructing an efficient scheme for computing the integrals with smooth integrands.

To evaluate the volume potentials numerically, we propose two schemes in the following two sections to handle domain integral in (2.5). One technique (ADS) is a modification of direct parameterization proposed in [8] for the linear system via adding a self-adaptive partition scheme with explicit quantitative criterion to discrete domain Ω . The other one is based on dual reciprocity method (DRM) [19] which transforms the domain integrals into equivalent boundary integrals without domain discretization.

3 Self-adaptive discretization for the volume potential

The standard technique for dealing with the volume potential in the linear system (2.17) is the domain parameterization which transforms the domain Ω into a standard rectangle domain Π , as proposed in [8]. Rather than the nonuniform domain partition of Ω derived by uniform domain discretization for Π in [8], here we propose a self-adaptive partition scheme (ADS) with explicit quantitative criterion to discrete domain Π , which ensures the integral in Ω can be computed numerically with uniform accuracy. Here we only give the scheme for $\Omega \subset \mathbb{R}^2$, the setting for $\Omega \subset \mathbb{R}^3$ is analogous, see numerics in section 5.

Assume that the domain Ω is star-like with the boundary curve $\partial\Omega$ and some center point $P_0 \in \Omega$. Then we can represent $\partial\Omega \in \mathbb{R}^2$ by

$$\partial\Omega := \{x(t) = (x_1(t), x_2(t)) = r(t)(\cos t, \sin t), t \in [0, 2\pi]\} + P_0,$$

with 2π -periodic radius function $r(t) > 0$. Now we introduce a one-to-one map between $\Pi := [0, 1] \times [0, 2\pi]$ and $\bar{\Omega}$ by

$$\tilde{p}(\eta, t) := p(\eta, t) + P_0 := (\eta x_1(t), \eta x_2(t)) + P_0 \in \bar{\Omega}$$

in the zero measure sense for the coordinate $(\eta, t) \in \Pi$, i.e.,

$$\tilde{p}|_{\{(\eta, t): (0,1) \times [0, 2\pi]\}} = \Omega \setminus \{P_0\}, \quad \tilde{p}|_{\{(0, t): t \in [0, 2\pi]\}} = P_0, \quad \tilde{p}|_{\{(1, t): t \in [0, 2\pi]\}} = \partial\Omega.$$

When establishing the solvability of the density pair (μ, ψ) in continuous function space, we need to restrict both the volume potential and the solution in arbitrarily specified interior domain Ω_{ϵ_0} by considering (2.5). However, the hyper-singularity of the operator $\mathbb{K}_{12}^{\partial\Omega \rightarrow \Omega}[\tilde{\psi}](x)$ for $x \in \Omega$ in discrete version can be removed numerically by taking $x \in \Omega$ in the kernel function with fixed positive distance to $\partial\Omega$. Consequently, instead of (2.5), we can still consider the system (2.17) directly for the numerical realizations, with the parameterized version

$$\begin{cases} (\mathbb{I} - \mathbb{K}_{11}^{\Omega \rightarrow \Omega})[\tilde{\mu}](\tilde{p}(\eta, t)) + \mathbb{K}_{12}^{\partial\Omega \rightarrow \Omega}[\tilde{\psi}](\tilde{p}(\eta, t)) = \frac{F(\tilde{p}(\eta, t))}{\sigma(\tilde{p}(\eta, t))}, & (\eta, t) \in \Pi \\ \mathbb{K}_{21}^{\Omega \rightarrow \partial\Omega}[\tilde{\mu}](\tilde{p}(1, t)) + (\mathbb{I} - \mathbb{K}_{22}^{\partial\Omega \rightarrow \partial\Omega})[\tilde{\psi}](\tilde{p}(1, t)) = -2f(\tilde{p}(1, t)), & t \in [0, 2\pi], \end{cases} \quad (3.1)$$

where the operators have the parametrized representations

$$\begin{cases} \mathbb{K}_{11}^{\Omega \rightarrow \Omega}[\tilde{\mu}](\tilde{p}(\eta, t)) & := \frac{1}{2\pi} \int_0^1 \int_0^{2\pi} K_{11}(\eta, t; \xi, \tau) \tilde{\mu}(\tilde{p}(\xi, \tau)) d\tau d\xi, & (\eta, t) \in \Pi \\ \mathbb{K}_{12}^{\partial\Omega \rightarrow \Omega}[\tilde{\psi}](\tilde{p}(\eta, t)) & := \frac{1}{2\pi} \int_0^{2\pi} K_{12}(\eta, t; \tau) \tilde{\psi}(\tilde{p}(1, \tau)) d\tau, & (\eta, t) \in \Pi \\ \mathbb{K}_{21}^{\Omega \rightarrow \partial\Omega}[\tilde{\mu}](\tilde{p}(1, t)) & := \frac{1}{2\pi} \int_0^1 \int_0^{2\pi} K_{21}(t; \xi, \tau) \tilde{\mu}(\tilde{p}(\xi, \tau)) d\tau d\xi, & t \in [0, 2\pi] \\ \mathbb{K}_{22}^{\partial\Omega \rightarrow \partial\Omega}[\tilde{\psi}](\tilde{p}(1, t)) & := \frac{1}{2\pi} \int_0^{2\pi} K_{22}(t; \tau) \tilde{\psi}(\tilde{p}(1, \tau)) d\tau, & t \in [0, 2\pi] \end{cases}$$

with the kernels

$$\begin{cases} K_{11}(\eta, t; \xi, \tau) & := \frac{(\tilde{p}(\xi, \tau) - \tilde{p}(\eta, t)) \cdot \nabla \ln \sigma(\tilde{p}(\eta, t))}{|\tilde{p}(\eta, t) - \tilde{p}(\xi, \tau)|^2} J(\xi, \tau), \\ K_{12}(\eta, t; \tau) & := \frac{\partial}{\partial \nu(\tau)} \left(\frac{(\tilde{p}(\eta, t) - \tilde{p}(1, \tau)) \cdot \nabla \ln \sigma(\tilde{p}(\eta, t))}{|\tilde{p}(\eta, t) - \tilde{p}(1, \tau)|^2} \right) |x'(\tau)|, \\ K_{21}(t; \xi, \tau) & := -\ln \frac{1}{|\tilde{p}(1, t) - \tilde{p}(\xi, \tau)|^2} J(\xi, \tau), \\ K_{22}(t; \tau) & := \frac{2\partial}{\partial \nu(\tau)} \left(\ln \frac{1}{|\tilde{p}(1, t) - \tilde{p}(1, \tau)|} \right) |x'(\tau)|, \end{cases}$$

where $J(\xi, \tau) := \xi x(\tau) \cdot \nu(\tau) |x'(\tau)|$ is the Jacobian determinant for the coordinated transform $p : \Pi \rightarrow \Omega$, with the unit outward normal direction $\nu(\tau) := \frac{(x'_2(\tau), -x'_1(\tau))}{|x'(\tau)|}$.

For the surface potential $\mathbb{K}_{22}^{\partial\Omega \rightarrow \partial\Omega}$, its kernel $K_{22}(t, \tau)$ is continuous with the representation

$$K_{22}(t, \tau) = \begin{cases} \frac{x''(t) \cdot \nu(t)}{|x'(t)|}, & t = \tau \\ \frac{2(x(t) - x(\tau)) \cdot \nu(x(\tau))}{|x(t) - x(\tau)|^2} |x'(\tau)|, & \text{elsewhere.} \end{cases} \quad (3.2)$$

For this domain transformation, it is easy to see that $\eta x(t) - \xi x(\tau) = 0$ if and only if $(\eta, t) = (\xi, \tau)$. Therefore, by introducing

$$G_1(\eta, t) := \nu(t) \cdot \nabla \ln \sigma(\tilde{p}(\eta, t)), \quad G_2(\eta, t) := \theta(t) \cdot \nabla \ln \sigma(\tilde{p}(\eta, t))$$

with unit tangential direction $\theta(t) := \frac{(x'_1(t), x'_2(t))}{|x'(t)|}$, the kernel $K_{11}(\eta, t; \xi, \tau)$ has the decomposition

$$K_{11}(\eta, t; \xi, \tau) \equiv K^{(11)}(\eta, t; \xi, \tau) + \frac{J(\xi, \tau) G_2(\eta, t)}{\eta} \frac{G_2(\eta, t)}{2|x'(\tau)|} \cot \frac{\tau - t}{2}, \quad (3.3)$$

where $K^{(11)}(\eta, t; \xi, \tau)$ is a continuous function with the representation

$$K^{(11)}(\eta, t; \xi, \tau) = \begin{cases} J(\eta, t) \left[G_1(\eta, t) \frac{x''(t) \cdot \nu(t)}{2\eta|x'(\tau)|^2} + G_2(\eta, t) \frac{x''(t) \cdot \theta(t)}{2\eta|x'(\tau)|^2} \right], & (\eta, t) = (\xi, \tau) \\ J(\xi, \tau) \left[G_1(\eta, t) \kappa_1(\eta, t; \xi, \tau) + G_2(\eta, t) \kappa_2(\eta, t; \xi, \tau) \right], & \text{elsewhere} \end{cases} \quad (3.4)$$

with

$$\begin{cases} \kappa_1(\eta, t; \xi, \tau) := \frac{(\xi x(\tau) - \eta x(t)) \cdot \nu(t)}{|\eta x(t) - \xi x(\tau)|^2}, \\ \kappa_2(\eta, t; \xi, \tau) := \frac{(\xi x(\tau) - \eta x(t)) \cdot \theta(t)}{|\eta x(t) - \xi x(\tau)|^2} - \frac{1}{2\eta|x'(\tau)|} \cot \frac{\tau - t}{2}. \end{cases}$$

The weak singular integrals in (3.3) with respect to τ can be computed using the standard formula [5]

$$\begin{cases} \frac{1}{2\pi} \int_0^{2\pi} g(\tau) \cot \frac{\tau - t}{2} d\tau \approx \sum_{j=0}^{2n-1} T_j(t; n) g(t_j), \\ \frac{1}{2\pi} \int_0^{2\pi} g(\tau) \ln \left(4 \sin^2 \frac{\tau - t}{2} \right) d\tau \approx \sum_{j=0}^{2n-1} F_j(t; n) g(t_j), \end{cases} \quad (3.5)$$

with the weight functions

$$\begin{cases} F_j(t; n) = -\frac{1}{n} \left[\sum_{m=1}^{n-1} \frac{1}{m} \cos m(t - t_j) + \frac{1}{2n} \cos n(t - t_j) \right], \\ T_j(t; n) = -\frac{1}{n} \sum_{m=1}^{n-1} \sin m(t - t_j) - \frac{1}{2n} \sin n(t - t_j) \end{cases} \quad (3.6)$$

for $t \in [0, 2\pi)$ and $j = 0, \dots, 2n - 1$.

Now we consider the volume potential with smooth integrands. The special techniques for computing the volume potentials $\mathbb{K}_{11}^{\Omega \rightarrow \Omega}$, $\mathbb{K}_{21}^{\Omega \rightarrow \partial\Omega}$ should be developed, notice the fact that, when we decompose the integral domain Ω into the summation of N -circle ring

$$\Omega_i := \{\tilde{p}(\xi, \tau) : (\xi, \tau) \in [\xi_{i-1}, \xi_i] \times [0, 2\pi]\} \subset \Omega$$

with $\xi_i := \frac{i}{N}$ for $i = 1, \dots, N$ along radius direction, the area of Ω_i will increase for large i , see Figure 1 for the geometric configuration. So we should introduce some self-adaptive rule to

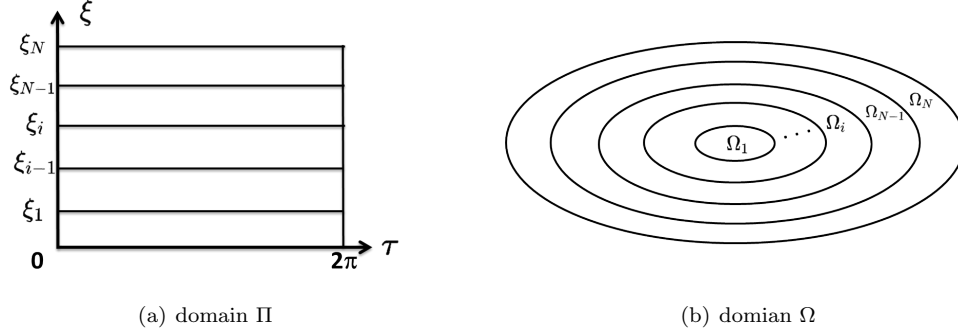


Figure 1: Π_i is transformed as Ω_i by $\Omega_i = \tilde{p}(\Pi_i)$.

compute the integrals in all Ω_i for keeping the uniform accuracy of the integral in Ω . That is, the integrals in Ω_i should be computed by different steps τ for different i .

For the grids $0 = \xi_0 < \xi_1 < \dots < \xi_N = 1$, we have the decomposition

$$\bar{\Omega} \equiv \bigcup_{i=1}^N \bar{\Omega}_i \equiv \bigcup_{i=1}^N \{\tilde{p}(\xi, \tau) : (\xi, \tau) \in \Pi_i := [\xi_{i-1}, \xi_i] \times [0, 2\pi]\}.$$

Remark 3.1. In the special case of Ω being an unit cycle, the area of each layer is

$$|\Omega_i| = \left(\frac{i}{N}\right)^2 \pi - \left(\frac{i-1}{N}\right)^2 \pi = \frac{2i-1}{N^2} \pi, \quad i = 1, \dots, N, \quad (3.7)$$

which increases linearly with respect to i .

To compute the integral in each Ω_i with higher accuracy, we introduce the closed curve $\{\tilde{p}(\xi_{i-1/2}, \tau) : \tau \in [0, 2\pi]\}$ with $\xi_{i-1/2} := (\xi_{i-1} + \xi_i)/2$ for $i = 1, \dots, N$. Inserting these middle lines $\xi = \xi_{i-1/2}$ into Π , the rectangle Π is double-partitioned as $2N$ rectangles with the grids

$$0 = \xi_0 < \xi_{1/2} < \xi_1 < \xi_{3/2} < \xi_2 \dots < \xi_{N-1} < \xi_{N-1/2} < \xi_N = 1.$$

Now we apply the middle-rectangle formula in Ω_0, Ω_N and the Simpson's formula in Ω_i for $i = 1, \dots, N-1$ to compute

$$\int_{\Omega_i} s(x) dx = \int_{\Pi_i} s(\tilde{p}(\xi, \tau)) J(\xi, \tau) d\xi d\tau := \int_{\xi_{i-1}}^{\xi_i} d\xi \int_0^{2\pi} s_J(\xi, \tau) d\tau$$

with $s_J(\xi, \tau) := s(\tilde{p}(\xi, \tau)) J(\xi, \tau)$. That is, we have

$$\int_{\Omega_i} s(x) dx \approx \begin{cases} \int_0^{2\pi} s_J(\xi_{i-1/2}, \tau) d\tau (\xi_i - \xi_{i-1}), & i = 1, N \\ \int_0^{2\pi} [s_J(\xi_{i-1}, \tau) + 4s_J(\xi_{i-1/2}, \tau) + s_J(\xi_i, \tau)] d\tau \frac{\xi_i - \xi_{i-1}}{6}, & i = 2, \dots, N-1, \end{cases}$$

which is rewritten as

$$\int_{\Omega_i} s(x) dx \approx \int_0^{2\pi} [\alpha_i^1 s_J(\xi_{i-1}, \tau) + \alpha_i^2 s_J(\xi_{i-1/2}, \tau) + \alpha_i^3 s_J(\xi_i, \tau)] d\tau \quad (3.8)$$

for $i = 1, \dots, N$ with

$$(\alpha_i^1, \alpha_i^2, \alpha_i^3) = \begin{cases} (\xi_i - \xi_{i-1})(0, 1, 0), & i = 1, N, \\ \frac{\xi_i - \xi_{i-1}}{6}(1, 4, 1), & i = 2, \dots, N-1. \end{cases} \quad (3.9)$$

In terms of (3.8), we need to compute the integrals $\int_0^{2\pi} s_J(\xi_i, \tau) d\tau$, $\int_0^{2\pi} s_J(\xi_{i-\frac{1}{2}}, \tau) d\tau$ for $i = 1, 2, \dots, N$. Define $\tilde{\xi}_i := \xi_{\frac{i}{2}}$ for $i = 1, 2, \dots, 2N$, see Figure 2.

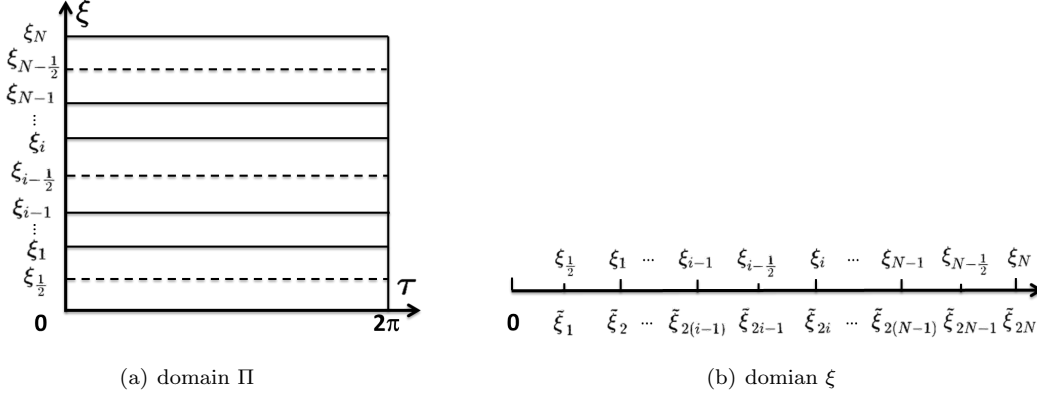


Figure 2: Refinement of the interval $[0, 1]$ as $2N$ subintervals and reordering the partition points.

Divide the segment $\{(\tilde{\xi}_i, \tau) : \tau \in [0, 2\pi]\}$ as $2n_i$ equi-intervals for $i = 1, \dots, 2N$, where we specify $n_1 = 2^{k_1}$ and $n_i = n_1 2^{k_i}$ with $k_i \in \mathbb{N}^+$ for $i = 2, \dots, 2N$. Then, based on the $2n_i + 1$ grids on $\{(\tilde{\xi}_i, \tau) : \tau \in [0, 2\pi]\}$, we divide the layer

$$\tilde{\Omega}_i := \{(\xi, \tau) \in [\tilde{\xi}_{i-1}, \tilde{\xi}_i] \times [0, 2\pi], i = 1, \dots, 2N\}$$

as the union of several triangles. In terms of the case either $n_i = n_{i-1}$ or $n_i = 2n_{i-1}$, there are two different partitions, namely, either the red partition or the black one, as shown in Figure 3.

Our criteria for specifying k_i is that the area of each triangle in $\tilde{\Omega}_i$ for $i = 2, \dots, 2N$ has almost the same size as the triangle in $\tilde{\Omega}_1$, see Figure 3(b). More precisely, we take the rule

$$|s_i| := \frac{|\tilde{\Omega}_i|}{2 \cdot 2n_i} \approx \frac{|\tilde{\Omega}_1|}{2n_1} := |s_1| \text{ or } |s_i| := \frac{|\tilde{\Omega}_i|}{3 \cdot 2n_i} \approx \frac{|\tilde{\Omega}_1|}{2n_1} := |s_1|, \quad (3.10)$$

which is specified for $i = 2, \dots, 2N$ from the quantitative rule

$$\frac{1}{3} \leq \frac{|s_i|}{|s_1|} \leq 3. \quad (3.11)$$

Using the grids $\{\tilde{\xi}_i : i = 1, \dots, 2N\}$ with $\tilde{\xi}_1 = \xi_{\frac{1}{2}}$ and $\tilde{\xi}_{2N} = \xi_N$ in (3.8) together with (3.9), it follows from the straightforward but lengthy computations that

$$\int_{\Omega} s(x) dx \equiv \sum_{i=1}^N \int_{\Omega_i} s(x) dx \approx \sum_{k=1}^{2N-1} c_k \int_0^{2\pi} s_J(\tilde{\xi}_k, \tau) d\tau \approx \sum_{k=1}^{2N-1} c_k \frac{2\pi}{2n_k} \sum_{j=0}^{2n_k-1} s_J(\tilde{\xi}_k, t_j^k), \quad (3.12)$$

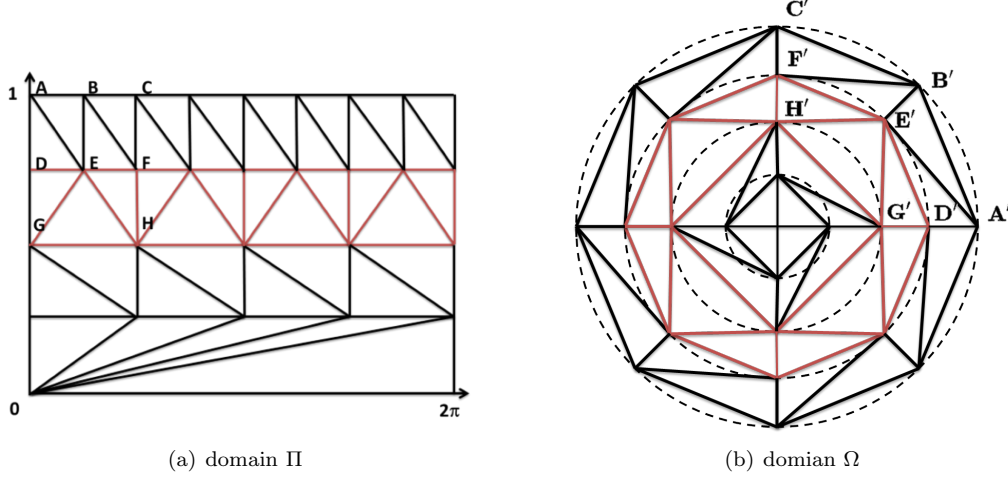


Figure 3: The adaptive partition scheme at each layer.

with $t_j^k := j \frac{\pi}{n_k}$ and the weights

$$c_{2i-1} = \begin{cases} \frac{1}{N}, & i = 1, N, \\ \frac{2}{3N}, & i = 2, \dots, N-1, \end{cases} \quad c_{2i} = \begin{cases} \frac{1}{6N}, & i = 1, N, \\ \frac{1}{3N}, & i = 2, \dots, N-2. \end{cases} \quad (3.13)$$

Since the area $\tilde{\Omega}_i$ is hard to compute for Ω of general shape, by employing (3.7) as a benchmark for $\tilde{\Omega}_i$ in (3.10) and (3.11), we finally take $k_i = \lfloor \log_2(2i-1) \rfloor$ for $i = 2, \dots, 2N$ with specified k_1 . For the concrete case $N = 10, k_1 = 3$, the step sizes with respect to τ from this self-adaptive strategy for different $\tilde{\xi}_i$ are presented in Table 1. It can be seen that partition numbers from the inner curve to the outer curve will become large.

Based on the decomposition (3.3), we apply (3.5) to compute the singular integrals and (3.12)-(3.13) to compute the regular ones in (3.3), which lead to the linear system

$$\begin{cases} \tilde{\mu}(\tilde{p}(\eta, t)) - \sum_{i=1}^{2N-1} c_i \sum_{j=0}^{2n_i-1} \hat{K}_{11}(\eta, t; \tilde{\xi}_i, t_j^i) \tilde{\mu}_{ij} + \sum_{j=0}^{2n_{2N}-1} \frac{1}{2n_{2N}} K_{12}(\eta, t; t_j^{2N}) \tilde{\psi}_j = \frac{F(\tilde{p}(\eta, t))}{\sigma(\tilde{p}(\eta, t))}, \\ \sum_{i=1}^{2N-1} c_i \frac{1}{2n_i} \sum_{j=0}^{2n_i-1} K_{21}(t; \tilde{\xi}_i, t_j^i) \tilde{\mu}_{ij} + \tilde{\psi}(\tilde{p}(1, t)) - \sum_{j=0}^{2n_{2N}-1} \frac{1}{2n_{2N}} K_{22}(t; t_j^{2N}) \tilde{\psi}_j = -2f(\tilde{p}(1, t)), \end{cases} \quad (3.14)$$

Table 1: The partition numbers at different layers from our self-adaptive strategy.

n_1	n_2	n_3	n_4	n_5	n_6	n_7	n_8	n_9	n_{10}
2^3	2^4	2^5	2^5	2^6	2^6	2^6	2^6	2^7	2^7
n_{11}	n_{12}	n_{13}	n_{14}	n_{15}	n_{16}	n_{17}	n_{18}	n_{19}	n_{20}
2^7	2^7	2^7	2^7	2^7	2^7	2^8	2^8	2^8	2^8

with the known coefficients

$$\hat{K}_{11}(\eta, t; \tilde{\xi}_i, t_j^i) := \frac{1}{2n_i} K^{(11)}(\eta, t; \tilde{\xi}_i, t_j^i) + \frac{J(\tilde{\xi}_i, t_j^i) G_2(\eta, t)}{\eta} \frac{1}{2|x'(t)|} T_j(t; n_i)$$

and the unknowns $\tilde{\mu}_{ij} := \tilde{\mu}(\tilde{p}(\tilde{\xi}_i, t_j^i))$, $\tilde{\psi}_j := \tilde{\psi}(\tilde{p}(1, t_j^{2N}))$.

By specifying (η, t) in (3.14) at the collocation points $(\tilde{\xi}_i, t_j^i)$ with $j = 0, \dots, 2n_i - 1, i = 1, \dots, 2N - 1$ in the first equation and $t = t_j^{2N}$ in the second equation, we can finally solve $\tilde{\mu}_{ij}$ for $j = 0, \dots, 2n_i - 1, i = 1, \dots, 2N - 1$ and $\tilde{\psi}_j$ for $j = 0, 1, \dots, 2N - 1$.

4 The dual reciprocity method

In the above section, we already propose a scheme dealing with the volume potential (2.5) by partitioning the domain Ω in some uniform way, which is still the realization of domain integral and consequently suffers from the large number of the unknowns $\{\tilde{\mu}_{i,j} : j = 0, 1, \dots, 2n_i - 1, i = 1, \dots, 2N - 1\}$ from the partition of Ω . In this section, we apply the dual reciprocity method (DRM) to transform the domain integral into boundary integral. One of the attractive feature of DRM is that the choice of interior nodes can be random and compute the weak singularity in the domain integral explicitly.

The essence of DRM is to transform the volume integral with fundamental solution as kernel function into a surface integral by expanding the integrand in terms of some base functions $\{f_k : k = 1, \dots, M\}$, and consequently decreases the number of grids for integration [19]. More precisely, we expand

$$\tilde{\mu}(x) \approx \sum_{k=1}^M \alpha_k f_k(x), \quad (4.1)$$

where $\{f_k(x) : k = 1, \dots, M\}$ constitutes the basis functions in the form

$$f_k(x) = \Delta \hat{f}_k(x) \quad (4.2)$$

for some known $\hat{f}_k(x)$ depending on interior nodes $x_k \in \Omega$ and α_k is the expansion coefficients to be determined. Substituting (4.2) and (4.1) into $\mathbb{K}_{11}^{\Omega \rightarrow \bar{\Omega}}[\tilde{\mu}](x)$ in (2.5) yields

$$\begin{aligned} \mathbb{K}_{11}^{\Omega \rightarrow \Omega}[\tilde{\mu}](x) &= \int_{\Omega} \nabla_x \Phi(x, y) \cdot \nabla \ln \sigma(x) \tilde{\mu}(y) dy \\ &\approx \sum_{k=1}^M \alpha_k \nabla_x \left(\int_{\Omega} \Phi(x, y) \Delta_y \hat{f}_k(y) dy \right) \cdot \nabla \ln \sigma(x), \quad x \in \Omega. \end{aligned} \quad (4.3)$$

Defining $D_k(x) := \int_{\Omega} \Phi(x, y) \Delta_y \hat{f}_k(y) dy$ and integrating by parts, we have

$$\begin{aligned} D_k(x) &= \int_{\partial\Omega} [\Phi(x, y) \partial_{\nu(y)} \hat{f}_k(y) - \hat{f}_k(y) \partial_{\nu(y)} \Phi(x, y)] ds(y) + \int_{\Omega} \hat{f}_k(y) \Delta_y \Phi(x, y) dy \\ &= \int_{\partial\Omega} [\Phi(x, y) \partial_{\nu(y)} \hat{f}_k(y) - \hat{f}_k(y) \partial_{\nu(y)} \Phi(x, y)] ds(y) - \hat{f}_k(x), \quad x \in \Omega. \end{aligned} \quad (4.4)$$

It is noted that $D_k(x)$ involves only boundary integral and the singularity in $\mathbb{K}_{11}^{\Omega \rightarrow \Omega}[\tilde{\mu}](x)$ has been integrated explicitly. Thus it is convenient to handle $\mathbb{K}_{11}^{\Omega \rightarrow \Omega}[\tilde{\mu}](x)$ numerically, since only the boundary discretization is required for specified \hat{f}_k in (4.2).

Similarly, the domain integral $\mathbb{K}_{21}^{\Omega \rightarrow \partial\Omega}[\tilde{\mu}](x)$ can also be converted into the boundary integral

$$\mathbb{K}_{21}^{\Omega \rightarrow \partial\Omega}[\tilde{\mu}](x) = -2 \int_{\Omega} \Phi(x, y) \tilde{\mu}(y) dy \approx -2 \sum_{k=1}^M \alpha_k D_k(x), \quad x \in \partial\Omega, \quad (4.5)$$

with $D_k(x)$ for $x \in \partial\Omega$ is defined by $D_k(x) := \lim_{z \in \Omega, z \rightarrow x} D_k(z)$, which is of the expression

$$\begin{aligned} D_k(x) &= \int_{\partial\Omega} [\Phi(x, y) \partial_{\nu(y)} \hat{f}_k(y) - \hat{f}_k(y) \partial_{\nu(y)} \Phi(x, y)] ds(y) + \int_{\Omega} \hat{f}_k(y) \Delta_y \Phi(x, y) dy \\ &= \int_{\partial\Omega} [\Phi(x, y) \partial_{\nu(y)} \hat{f}_k(y) - \hat{f}_k(y) \partial_{\nu(y)} \Phi(x, y)] ds(y) - \frac{1}{2} \hat{f}_k(x), \quad x \in \partial\Omega \end{aligned} \quad (4.6)$$

due to the jump relation of surface potentials. The boundary integrals with $\Phi(x, y)$ and $\partial_{\nu(y)} \Phi(x, y)$ being kernels can be computed from standard formulas.

Since we transform all the domain integrals in the linear system into boundary integrals via DRM, the numerical solution of the boundary value problem (1.1) can be generated conveniently, since the linear system for the density functions involves only the values on the boundary grids. Such a scheme will decrease the computational cost, especially in 3-dimensional cases.

Now we compute $\mathbb{K}_{11}^{\Omega \rightarrow \Omega}[\tilde{\mu}](x)$ for $x \in \Omega$ and $\mathbb{K}_{21}^{\Omega \rightarrow \partial\Omega}[\tilde{\mu}](x)$ for $x \in \partial\Omega$ by (4.3) and (4.5) in terms of the expression $D(x)$.

Here we only give the scheme for the case $\Omega \subset \mathbb{R}^2$, where the Nyström scheme can be used to construct the quadrature rules for boundary integrals. As for the case $\Omega \subset \mathbb{R}^3$, the discrete scheme stated in [20] (Chapter 3.7) can be applied to handle the singularities and build an efficient scheme for computing the integrals with smooth integrals. In section 5, a numerical example showing this methodology will be presented.

Assume that the boundary curve $\partial\Omega$ has a 2π -periodic parametric representation

$$\tilde{x}(t) := x(t) + P_0 \in \partial\Omega, \quad 0 \leq t \leq 2\pi.$$

Introduce the quadrature points $t_j = \pi j/n, j = 0, 1, \dots, 2n-1$ for boundary curve $\{\tilde{x}(t) : t \in [0, 2\pi]\}$. Since $\nabla D_k(x) \cdot \nabla \ln \sigma(x)$ with $D_k(x)$ given by (4.4) has smooth kernel function, the discrete version of $\mathbb{K}_{11}^{\Omega \rightarrow \Omega}[\tilde{\mu}](x)$ for $x \in \Omega$ in terms of Nyström is [20]

$$\mathbb{K}_{11}^{\Omega \rightarrow \Omega}[\tilde{\mu}](x) \approx \sum_{k=1}^M \alpha_k \left[\sum_{j=1}^{2n} \frac{1}{2n} \left(\tilde{G}_j(x) \hat{q}_{jk} - \tilde{H}_j(x) |x'(t_j)| \hat{f}_{jk} \right) - \nabla \hat{f}_k(x) \cdot \nabla \ln \sigma(x) \right] \quad (4.7)$$

for $x \in \Omega$, where $\hat{f}_{jk} = \hat{f}_k(y_j)$, $\hat{q}_{jk} = |x'(t_j)| \partial_{\nu(y)} \hat{f}_k(y) \Big|_{y=y_j}$ with $y_j = \tilde{x}(t_j)$ and

$$\tilde{G}_j(x) = \frac{(x - y_j) \cdot \nabla \ln \sigma(x)}{|x - y_j|^2} \quad \tilde{H}_j(x) = \frac{\partial}{\partial \nu(y)} \left(\frac{(x - y) \cdot \nabla \ln \sigma(x)}{|x - y|^2} \right) \Big|_{y=y_j}$$

For computing (4.5) with logarithmic singularity in $D_k(x)$ for $x \in \partial\Omega$, we firstly make the decomposition

$$\begin{aligned}
& -2D_k(\tilde{x}(t)) \\
&= \frac{1}{2\pi} \int_0^{2\pi} \left[\ln |x(t) - x(\tau)|^2 \partial_{\nu(\tilde{x}(\tau))} \left(\hat{f}_k(\tilde{x}(\tau)) \right) |x'(\tau)| + \hat{f}_k(\tilde{x}(\tau)) K_{22}(t; \tau) \right] d\tau + \hat{f}_k(\tilde{x}(t)) \\
&= \frac{1}{2\pi} \int_0^{2\pi} \left[\ln \frac{|x(t) - x(\tau)|^2}{4 \sin^2 \frac{t-\tau}{2}} + \ln \left(4 \sin^2 \frac{t-\tau}{2} \right) \right] |x'(\tau)| \partial_{\nu(\tilde{x}(\tau))} \left(\hat{f}_k(\tilde{x}(\tau)) \right) d\tau + \\
& \quad \frac{1}{2\pi} \int_0^{2\pi} K_{22}(t, \tau) \hat{f}_k(\tilde{x}(\tau)) d\tau + \hat{f}_k(\tilde{x}(t)), \quad 0 \leq t \leq 2\pi,
\end{aligned}$$

which leads to for $\tilde{x} \in \partial\Omega$ that

$$\mathbb{K}_{21}^{\Omega \rightarrow \partial\Omega}[\tilde{\mu}](\tilde{x}(t)) \approx \sum_{k=1}^M \alpha_k \left[\sum_{j=1}^{2n} \left(G_j(\tilde{x}(t)) \hat{q}_{jk} + \frac{1}{2n} K_{22}(t, t_j) \hat{f}_{jk} \right) + \hat{f}_k(\tilde{x}(t)) \right], \quad (4.8)$$

where $G_j(\tilde{x}(t))$ is a continuous function

$$G_j(\tilde{x}(t)) = F_j(t; n) + \begin{cases} \frac{1}{2n} \ln(|x'(t)|^2), & t = t_j \\ \frac{1}{2n} \ln \frac{|x(t) - x(t_j)|^2}{4 \sin^2 \frac{t-t_j}{2}}, & \text{elsewhere} \end{cases}$$

with $F_j(t; n)$ defined in (3.6). Finally we yield the following approximate version of (2.5):

$$\begin{cases} \sum_{k=1}^M \alpha_k f_k(x) - \sum_{k=1}^M \alpha_k DK_{11}(x; k) - \sum_{j=1}^{2n} \frac{1}{2n} \tilde{H}_j(x) |x'(t_j)| \tilde{\psi}_j = \frac{F(x)}{\sigma(x)}, \\ \sum_{k=1}^M \alpha_k DK_{21}(t; k) + \tilde{\psi}(\tilde{x}(t)) - \sum_{j=1}^{2n} \frac{1}{2n} K_{22}(t; t_j) \tilde{\psi}_j = -2f(\tilde{x}(t)) \end{cases} \quad (4.9)$$

with respect to the unknowns $\alpha_k (k = 1, \dots, M)$ and $\tilde{\psi}_j := \tilde{\psi}(\tilde{x}(t_j)) (j = 1, \dots, 2n)$, where the known coefficients

$$\begin{aligned}
DK_{11}(x; k) &= \sum_{j=1}^{2n} \frac{1}{2n} \left(\tilde{G}_j(x) \hat{q}_{jk} - \tilde{H}_j(x) |x'(t_j)| \hat{f}_{jk} \right) - \nabla \hat{f}_k(x) \cdot \nabla \ln \sigma(x), \\
DK_{21}(t; k) &= \sum_{j=1}^{2n} \left(G_j(\tilde{x}(t)) \hat{q}_{jk} + \frac{1}{2n} K_{22}(t, t_j) \hat{f}_{jk} \right) + \hat{f}_k(\tilde{x}(t)).
\end{aligned}$$

By specifying (x, t) in (4.9) at the collocation points (x_k, t_j) with $k = 1, \dots, M$ and $j = 1, \dots, 2n$, we can finally solve α_k for $k = 1, \dots, M$ and $\tilde{\psi}_j$ for $j = 1, \dots, 2n$. Finally the density function $\tilde{\mu}(x)$ can be approximated by (4.1).

The expansion of density $\tilde{\mu}(x)$ needs to specify the basis function $f_k(x)$. Since $\tilde{f}_k(x)$ is required to meet $\Delta \tilde{f}_k(x) = f_k(x)$, it is convenient to choose $f_k(x)$ in some special form. For specified internal grid $x_k \in \Omega \subset \mathbb{R}^d$, as recommended in [21], a typical form is

$$f_k(x) = 1 + r_k(x) := 1 + |x - x_k|, \quad k = 1, \dots, M, \quad (4.10)$$

where $r_k(x)$ is the distance between the field point x and the internal grid x_k .

For radial basis function f_k in this form, we also find the radial basis function $\hat{f}_k(x) := \hat{f}(r_k)$ to (4.2), which satisfies the ordinary differential equation [21]

$$\frac{d^2 \hat{f}}{dr_k^2} + \frac{d-1}{r_k} \frac{d\hat{f}}{dr_k} = 1 + r_k.$$

One solution to this equation is

$$\hat{f}_k(x) = \begin{cases} \frac{r_k^2(x)}{4} + \frac{r_k^3(x)}{9}, & d = 2, \\ \frac{r_k^2(x)}{6} + \frac{r_k^3(x)}{12}, & d = 3. \end{cases} \quad (4.11)$$

Then the derivatives $\partial_{\nu(x)} \hat{f}_k(x), \nabla \hat{f}_k(x)$ can be computed easily.

5 Numerical experiments

Now we do numerics for solving (1.1) by our proposed schemes for two examples in $\Omega \subset \mathbb{R}^d$, showing the validity of our proposed schemes. Moreover, we also compare the numerical performances of two schemes.

Example 1. Consider two different domains $\Omega \subset \mathbb{R}^2$. One is a heart-shaped domain with

$$\partial\Omega := \Gamma \equiv \{x(t) = (0.2 \cos t, 0.4 \sin t - 0.3 \sin^2 t), t \in [0, 2\pi]\} + (0.5, 1), \quad (5.1)$$

and the other one is an elliptical domain with

$$\partial\Omega := \Gamma \equiv \{x(t) = (\cos t, 0.5 \sin t), t \in [0, 2\pi]\} + (0.5, 1), \quad (5.2)$$

that is, we always take $P_0 = (0.5, 1)$ as the center of domain Ω . For the conductivity

$$\sigma(x, y) = 2 + \frac{1}{5} \sin(25x) + \frac{1}{5} \cos(25y)$$

and the source function

$$F(x, y) = -10[x \cos(25x) + \sin(25y)] - [4 + \frac{2}{5} \sin(25x) + \frac{2}{5} \cos(25y)]$$

in $\Omega \subset \mathbb{R}^2$, it is easy to verify that $u_{ex}(x, y) = x^2 - 2y + 3$ is the exact solution to the PDE in (1.1). Correspondingly, we take $f(x, y) = u_{ex}(x, y)|_{\partial\Omega}$ as the boundary value in (1.1).

1A: Realization of ADS in section 3.

For the discretization of Ω along radial direction, we divide $[0, 1]$ for ξ as 20 subintervals in (ξ, τ) coordinates by setting $N = 10$. Then the outer boundary of Ω_i has the representation

$$\Gamma_i := \{\tilde{\xi}_i x(t) : t \in [0, 2\pi]\} + (0.5, 1) \quad (5.3)$$

with $\tilde{\xi}_i = i \times \frac{1}{20}$ for $i = 1, \dots, 20$. To check the numerical performances, we consider the error of numerical solution in each curve $\Gamma_i \in \Omega$ (local error) and the whole domain Ω (average error)

by introducing the relative error functions

$$\frac{\|u_{Nn} - u_{ex}\|_{L^2(\Gamma_i)}}{\|u_{ex}\|_{L^2(\Gamma_i)}} \approx Err_L^i := \left(\frac{\sum_{j=0}^{2n_i-1} (u_{Nn} - u_{ex})^2(\tilde{\xi}_i, t_j^i) |\tilde{\xi}_i x'(t_j^i)|}{\sum_{j=0}^{2n_i-1} u_{ex}^2(\tilde{\xi}_i, t_j^i) |\tilde{\xi}_i x'(t_j^i)|} \right)^{1/2}, \quad (5.4)$$

$$\frac{\|u_{Nn} - u_{ex}\|_{L^2(\Omega)}}{\|u_{ex}\|_{L^2(\Omega)}} \approx Err_A := \left(\frac{\sum_{i=1}^{2N-1} \frac{c_i}{n_i} \sum_{j=0}^{2n_i-1} (u_{Nn} - u_{ex})^2(\tilde{\xi}_i, t_j^i) J(\tilde{\xi}_i, t_j^i)}{\sum_{i=1}^{2N-1} \frac{c_i}{n_i} \sum_{j=0}^{2n_i-1} u_{ex}^2(\tilde{\xi}_i, t_j^i) J(\tilde{\xi}_i, t_j^i)} \right)^{1/2} \quad (5.5)$$

respectively.

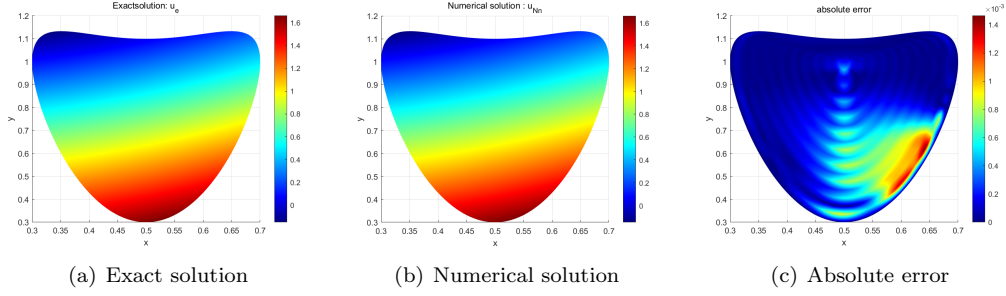


Figure 4: Numerical result for Example 1 in heart-shaped domain with $N = 10, k_1 = 3$.

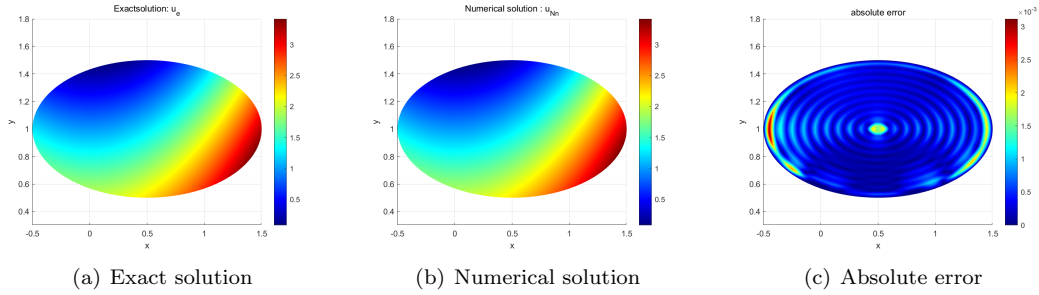


Figure 5: Numerical result for Example 1 in elliptical domain with $N = 10, k_1 = 3$.

The results in two different domains specified by (5.1) and (5.2) are illustrated in Figure 4 and Figure 5, where the columns (a),(b),(c) show the exact solution, numerical solution from our ADS, as well as the point-wise error distributions, respectively. It can be seen that ADS proposed in section 3 can yield numerical solution to a very satisfactory level. An interesting observation is that the maximum error always appears in the center area of Ω near P_0 and boundary curve Γ , the reason is that we always take a cycle Ω_1 without any further partition inside Ω_1 and Ω_{2N} . Also, when we compute the integrals in Ω_1 and Ω_{2N} , as shown in (3.9) for $i = 1, N$, only the middle-point rectangle quadrature formula are applied, rather than the Simpson's formula.

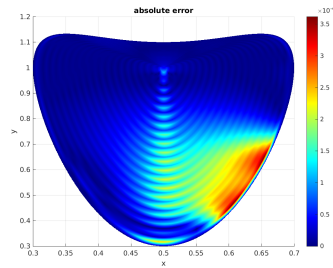
To describe the error distributions in Ω precisely, which cannot be observed from Figure 4 and Figure 5, we give a quantitative description in Table 2 and Table 3 for two different domains, where we choose four different curves $\Gamma_2, \Gamma_7, \Gamma_{12}, \Gamma_{17}$ inside two domains to show the local error distributions, and also the relative error in Ω for the average error. For these numerics, we test our scheme for $k_1 = 1, 2, 3$, which means the curve Γ_1 is divided as $2n_1 = 2 \times 2^{k_1}$ sub-intervals along τ directions. For other curves Γ_i with $i = 1, \dots, 20$, the step sizes with respect to τ are $2n_i = 2 \times n_1 2^{k_i}$, where we take $k_i = \lfloor \log_2(2i - 1) \rfloor$.

Table 2: Relative error for Example 1 in heart-shaped domain.

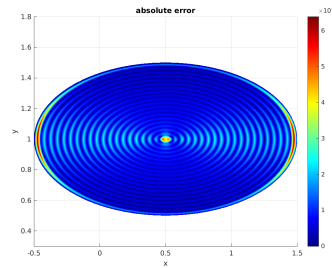
k_1	1	2	3
Err_L^2	4.56500×10^{-3}	1.14630×10^{-3}	0.32475×10^{-3}
Err_L^7	6.62500×10^{-3}	1.67670×10^{-3}	0.38854×10^{-3}
Err_L^{12}	7.03540×10^{-3}	1.57700×10^{-3}	0.38128×10^{-3}
Err_L^{17}	12.4350×10^{-3}	1.89370×10^{-3}	0.51314×10^{-3}
Err_A	10.3731×10^{-3}	4.52940×10^{-3}	0.51072×10^{-3}

Table 3: Relative error for Example 1 in elliptical domain.

k_1	1	2	3
Err_L^2	1.63660×10^{-3}	1.68310×10^{-3}	1.63660×10^{-3}
Err_L^7	4.12310×10^{-3}	1.22140×10^{-3}	1.21280×10^{-3}
Err_L^{12}	3.59170×10^{-3}	0.39568×10^{-3}	0.25058×10^{-3}
Err_L^{17}	4.99230×10^{-3}	0.66747×10^{-3}	0.51239×10^{-3}
Err_A	1.52940×10^{-3}	1.10763×10^{-3}	0.86416×10^{-3}



(a) Error for domain (5.1).



(b) Error for domain (5.2).

Figure 6: Error distributions for Example 1 by refinement of Ω with $N = 20, k_1 = 4$.

When we check the error distributions in Ω shown in Table 2 and Table 3, it can be seen

that the error in all different closed curves Γ_i and also the average error in the whole domain is always of the same amplitude $O(10^{-3})$, which reveal our uniform accuracy in the whole domain due to our self-adaptive partition strategy ADS in different Γ_i .

In the above implementations, we divide the domain Ω by the ξ -interval $[0, 1]$ for fixed $N = 10$ and $k_1 = 1, 2, 3$ dividing $\partial\Omega_1$ which also determines the partition size of Ω . It is imaginable that the computation accuracy will be improved if we refine the grids of the domain Ω , as shown in Figure 6 for two domains specified by (5.1) and (5.2), where the absolute errors are improved to $O(10^{-4})$.

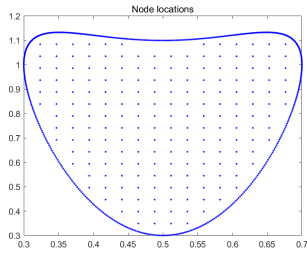
1B: Realization of DRM in section 4.

In order to represent the accuracy of the solution by the DRM proposed in section 4, we define a mean absolute error and a mean root square relative error by

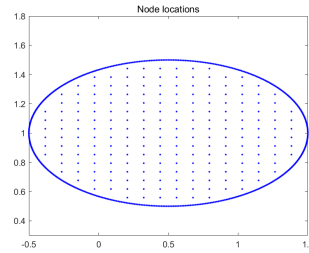
$$Err_m : \equiv \frac{1}{J} \sum_{j=1}^J |u_{Nn}(x_j) - u_{ex}(x_j)|, \quad (5.6)$$

$$Err_s : \equiv \left(\frac{\sum_{j=1}^J |u_{Nn}(x_j) - u_{ex}(x_j)|^2}{\sum_{j=1}^J |u_{ex}(x_j)|^2} \right)^{1/2}, \quad (5.7)$$

respectively, where $\{x_j : j = 1, \dots, J\} \subset \Omega$ is the set of internal nodes, $u_{Nn}(x_j)$ and $u_{ex}(x_j)$ are the numerical solution and exact one in the grid x_j , respectively. The distribution of internal nodes and boundary ones are presented in Figure 7.



(a) Node locations for domain (5.1).



(b) Node locations for domain (5.2).

Figure 7: Nodes distribution: (a) 196 internal nodes and 512 boundary nodes for domain (5.1); (b) 208 internal nodes and 512 boundary nodes for domain (5.2).

We compare the numerical performances of the DRM with the well-known FEM scheme. Since our proposed scheme is of 708 collocation nodes for domain (5.1) and 720 collocation nodes for domain (5.2) shown in Figure 7, we apply 717 nodes for domain (5.1) and 731 nodes for (5.2) to generate meshes in PDETOOL by Matlab for using FEM scheme, see (b) and (e) in Figure 8.

Under these discretizations with almost the same grids, our proposed DRM scheme is compatible with FEM. Figure 8 illustrates the results for two domains by DRM and the FEM

in MATLAB. The left column of Figure 8 shows the point-wise error distributions from our scheme, while the point-wise error for FEM is presented in the right column of Figure 8. It can be seen that the maximum errors of our scheme for two domains are always smaller than those of FEM for this example.

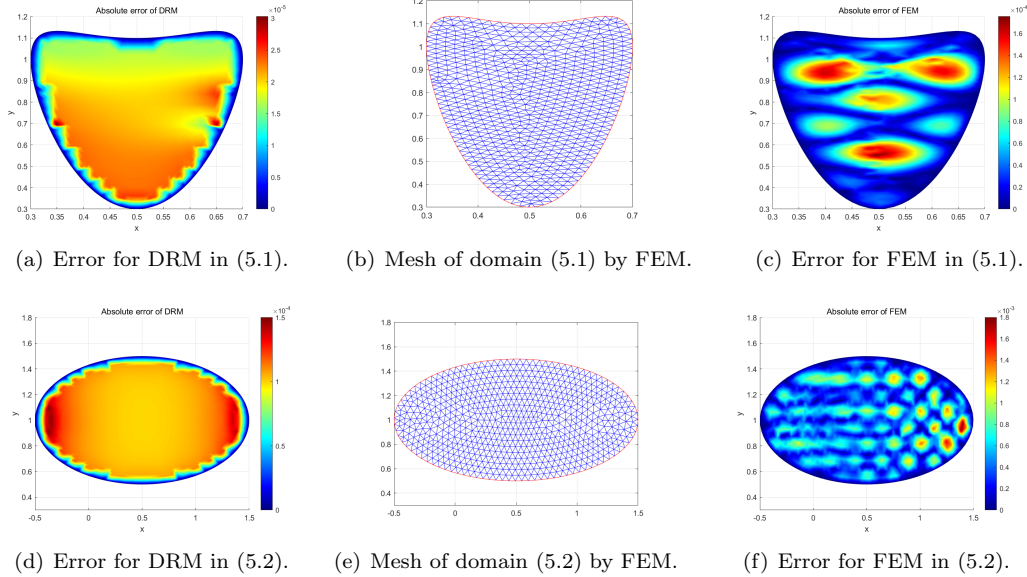


Figure 8: Numerical results of DRM and FEM in two domains.

Table 4: Numerics comparison for Example 1 in heart-shaped domain.

	Num_C	Err_m	Err_s	$Time$
ADS	856	2.3569×10^{-3}	3.9884×10^{-3}	1.28768 s
DRM	708	2.0243×10^{-5}	1.1663×10^{-5}	0.03191 s
FEM	717	5.3564×10^{-5}	8.1742×10^{-5}	0.48435 s

Now we compare the numerical performances of our proposed schemes ADS and DRM with FEM in the whole domain Ω in terms of average errors (5.6) and (5.7), instead of the point-wise error shown in Figure 8. Table 4 and Table 5 present (Err_m, Err_s) of our schemes and FEM for domain (5.1), domain (5.2), respectively, where Num_C is the number of collocation nodes. It can be revealed that, even if ADS chooses more nodes (856), the accuracy ($O(10^{-3})$) is still lower than DRM and FEM, with longer computational time. However, our second scheme DRM is of the same error order as FEM for compatible collocation nodes. For domain (5.2), Err_s of DRM ($O(10^{-5})$) is even lower than that for FEM ($O(10^{-4})$), as displayed in Table 5. It should be noted that our proposed scheme DRM takes less computational time than FEM,

Table 5: Numerics comparison for Example 1 in elliptical domain.

	Num_C	Err_m	Err_s	$Time$
ADS	856	4.3969×10^{-3}	3.6247×10^{-3}	1.36882 s
DRM	720	1.0902×10^{-4}	6.6762×10^{-5}	0.03326 s
FEM	731	5.0242×10^{-4}	6.6272×10^{-4}	0.47564 s

since mesh-generation of FEM is also time-consuming. However, DRM is a mesh-free scheme which chooses internal nodes randomly.

We further investigate the computational accuracy of DRM in terms of the number of internal grids. To this end, we keep the boundary grids unchanged but take different internal grids, as shown in Figure 9 and Figure 10, where there are approximately 10, 15, 20, 30 and 40 internal grids for two domains. Such a configuration approximates density function $\tilde{\mu}$ by very few grids. We present the errors for u in Table 6 and Table 7, where Num_I is the number of internal nodes.

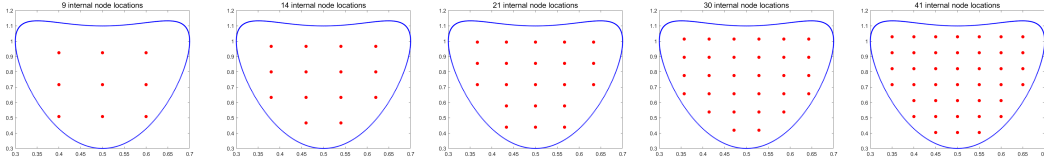


Figure 9: Different internal nodes distributions for domain (5.1).

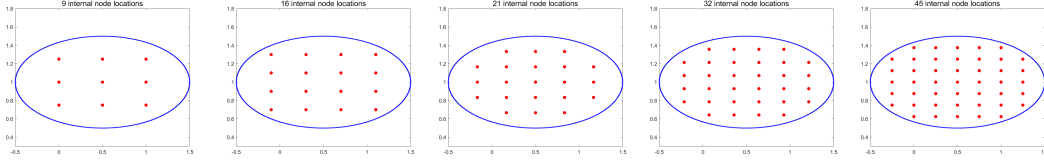


Figure 10: Different internal nodes distributions for domain (5.2).

Table 6: Error for Example 1 in heart-shaped domain.

Num_I	9	14	21	30	41
Err_m	2.007×10^{-4}	9.061×10^{-5}	4.702×10^{-5}	3.323×10^{-5}	2.496×10^{-5}
Err_s	6.213×10^{-4}	6.818×10^{-5}	3.380×10^{-5}	2.234×10^{-5}	1.564×10^{-5}

Table 7: Error for Example 1 in elliptical domain.

Num_I	9	16	21	32	45
Err_m	1.570×10^{-3}	5.539×10^{-4}	4.683×10^{-4}	2.008×10^{-4}	1.396×10^{-4}
Err_s	1.231×10^{-3}	4.970×10^{-4}	3.672×10^{-4}	1.762×10^{-4}	1.095×10^{-4}

From Table 6 and Table 7, it can be seen that our proposed DRM scheme can also yield satisfactory results which are good approximations to the exact solutions, even if we apply very few internal grids. For example, for 9 internal grids, the mean absolute errors are $O(10^{-4})$ and $O(10^{-3})$ for (5.1) and (5.2) respectively, while the root mean square relative errors are $O(10^{-4})$ and $O(10^{-3})$, which are satisfactory for the numerics of our boundary value problem.

From Table 4 and Table 5 for 2-dimensional domain Ω , ADS needs to apply a large number of points and consequently spends longer time to achieve satisfactory accuracy. Therefore, in the following 3-dimensional example, we only consider DRM for numerical realizations.

Example 2. A 3-dimensional model.

We take a pinched ball to be $\Omega \subset \mathbb{R}^3$ for finding our solution u , with the boundary surface

$$\partial\Omega = \{r(\theta, \varphi)x(\theta, \varphi) : x(\theta, \varphi) = (\sin \theta \cos \varphi, \sin \theta \sin \varphi, \cos \theta) \in \mathbb{S}^2, \theta \in [0, \pi], \varphi \in [0, 2\pi]\},$$

where $r(\theta, \varphi) = \sqrt{(1.44 + 0.5 \cos 2\varphi(\cos 2\theta - 1))}$, see Figure 11 for the geometric configuration.

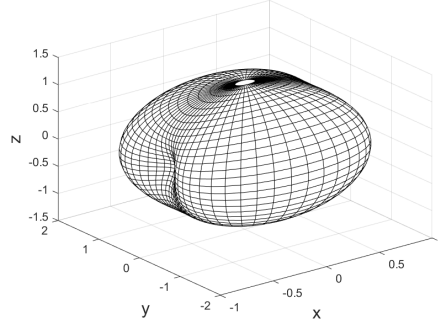


Figure 11: Geometric shape for the pinched ball Ω .

We give the conductivity in Ω as

$$\sigma(x, y, z) = x^2y + 2(y + z^2) + 2$$

and the internal source function

$$F(x, y, z) = -(6y + 2z)x^2 - 8yz - 4y - 20z - 4z^2 - 4.$$

Then $u_{ex}(x, y, z) = x^2 + 2(y+2)z + 1$ is the exact solution to (1.1) for corresponding $f \equiv u|_{\partial\Omega}$.

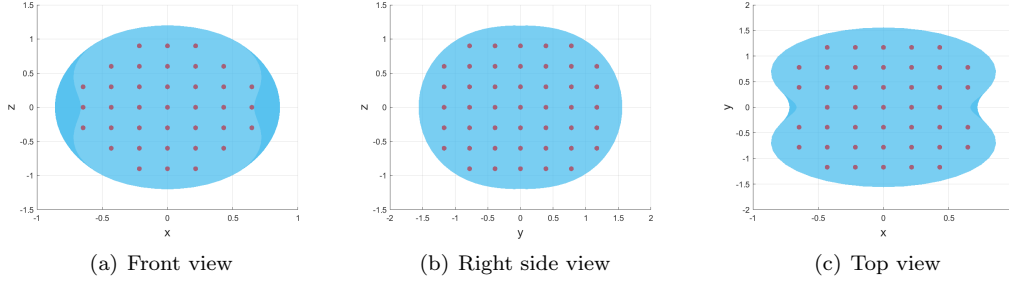


Figure 12: Three views of 197 equally spaced internal nodes for Ω .

We choose a set of quadrature nodes x_{jk} on the unit sphere \mathbb{S}^2 in terms of the polar coordinates by [20]

$$x_{jk} := (\sin \theta_j \cos \varphi_k, \sin \theta_j \sin \varphi_k, \cos \theta_j), \quad j = 1, \dots, N, \quad k = 0, \dots, 2N - 1,$$

where $\theta_j = \arccos t_j$, $\varphi_k = \pi k/N$ for the Gauss points t_j in $[-1, 1]$. Then we obtain $2N^2$ surface nodes $q_{jk} := r(\theta_j, \varphi_k)x_{jk} \in \partial\Omega$. As for internal nodes for Ω , we take 197 points equally spaced in Ω , the distribution in Ω from three views is shown in Figure 12.

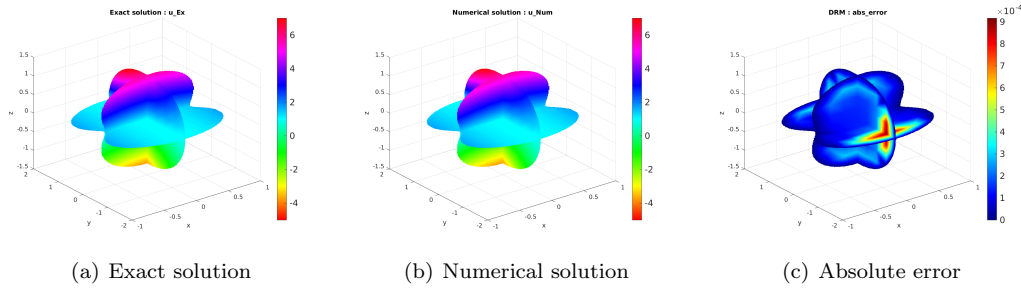


Figure 13: Numerical results for Example 2 with $N = 64$.

In Figure 13, we show the numerical performances of our DRM scheme with $N = 64$ at three slice planes orthogonal to x, y, z axis, respectively. The maximum absolute error is 9.1935×10^{-4} , while the mean absolute error Err_m and mean root square relative error Err_s defined by (5.6), (5.7) are 2.3467×10^{-4} and 1.2059×10^{-4} . It can be observed that our DRM scheme based on the Levi function representation can solve 3-dimensional problems with satisfactory numerical performances, including accuracy and computational cost. On the other hand, the larger errors are generally appear near to the boundary $\partial\Omega$. This phenomenon may be due to the effect of singularity of fundamental solution for Laplacian equation at those nodes.

In order to test the influence of the number of internal nodes, we consider the configurations of 15, 27, 79, 136—internal nodes for three set of surface nodes ($N = 16, 32, 64$). The internal nodes locations are shown in Figure 14 from the top view. We compute the density pair $(\tilde{\mu}, \tilde{\psi})$ at these relatively few nodes and then compute $u(x, y, z)$ in the whole domain Ω in terms of

the Levi function representation. The results are shown in Table 8 for different configurations of boundary and internal nodes, in terms of the error distributions and computational time.

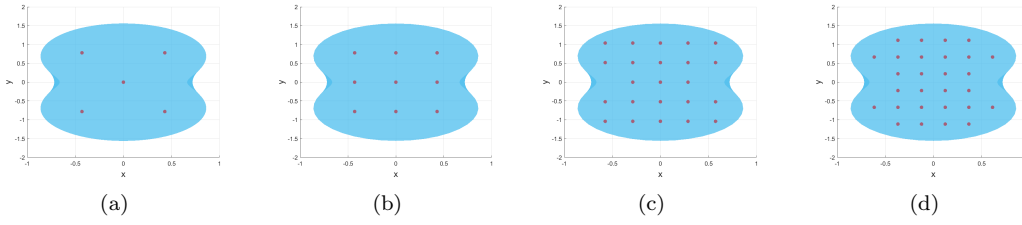


Figure 14: Different internal nodes from top view: (a) 15 internal nodes; (b) 27 internal nodes; (c) 79 internal nodes; (d) 136 internal nodes.

Table 8: Errors and computational time of Example 2 for different configurations.

	Num_I	15	27	79	136
N=16	Err_m	1.5424×10^{-2}	1.2205×10^{-2}	1.0253×10^{-2}	0.9422×10^{-2}
	Err_s	1.3823×10^{-2}	1.3128×10^{-2}	1.2035×10^{-2}	1.2364×10^{-2}
	$Time$	0.9240 s	0.9737 s	1.1476 s	1.5368 s
N=32	Err_m	2.7741×10^{-3}	1.8511×10^{-3}	5.1004×10^{-4}	3.5751×10^{-4}
	Err_s	1.5346×10^{-3}	1.0089×10^{-3}	3.1122×10^{-4}	2.4034×10^{-4}
	$Time$	61.285 s	61.918 s	73.720 s	90.568s
N=64	Err_m	2.3722×10^{-3}	1.8523×10^{-3}	4.9840×10^{-4}	3.1304×10^{-4}
	Err_s	1.3361×10^{-3}	1.0025×10^{-3}	2.8860×10^{-4}	1.7465×10^{-4}
	$Time$	2701.6 s	2720.5 s	2853.7 s	2855.8 s

From Table 8, it can be seen that for $N = 16$, the computation time is shortest but the accuracy is the lowest ($O(10^{-2})$). For $N = 32, 64$, all the numerical results are very close to exact solution with satisfactory error levels. Even for 15 internal nodes, the mean absolute error and mean root square relative error are up to $O(10^{-3})$. Comparing the results for $N = 32$ and $N = 64$, the errors are very close, but the computational time is quite different. Consequently, we can apply relatively few boundary and internal nodes by our DRM scheme to get satisfactory numerical results.

Acknowledgements: This work is supported by NSFC (No.11971104).

References

- [1] L.C. Evans, Partial Differential Equations, Amer. Math. Soc., 2010.
- [2] G.C. Hsiao, W.L. Wendland, Boundary Integral Equations, Springer-Verlag, Berlin, 2008.

- [3] R. Chapko, B.T. Johansson, On the numerical solution of a Cauchy problem for the Laplace equation via a direct integral equation approach, *Inverse Probl. Imaging*, Vol.6, No.1, 25-38, 2012.
- [4] R. Chapko, B.T. Johansson, A boundary integral equation method for numerical solution of parabolic and hyperbolic Cauchy problems, *Appl. Numer. Math.*, Vol.129, 104-119, 2018.
- [5] D. Colton, R. Kress, *Inverse Acoustic and Electromagnetic Scattering Theory*, Springer-Verlag, Berlin Heidelberg, 1992.
- [6] A. Pomp, *The Boundary-Domain Integral Method for Elliptic Systems with an Application to Shells*, *Lecture Notes in Mathematics*, Vol.1683, Springer, Berlin, 1998.
- [7] C.M. Miranda, *Partial Differential Equations of Elliptic Type*, Springer, 2nd Ed., 1970.
- [8] A. Beshley, R. Chapko, B.T. Johansson, An integral equation method for the numerical solution of a Dirichlet problem for second-order elliptic equations with variable coefficients, *J. Engrg. Math.*, Vol.112, 63-73, 2018.
- [9] S.E. Mikhailov, Analysis of united boundary-domain integro-differential and integral equations for a mixed BVP with variable coefficient, *Math. Meth. Appl. Sci.*, Vol.29, No.6, 715-739, 2006.
- [10] D. Nardini and C.A. Brebbia, A new approach for free vibration analysis using boundary elements, in *Boundary Element Methods in Engineering*, C.A. Brebbia, ed., Springer, Berlin, 312-326, 1982.
- [11] X.W. Gao, A boundary element method without internal cells for two-dimensional and three-dimensional elastoplastic problems, *J. Appl. Mech.*, Vol.69, 154-160, 2002.
- [12] W.T. Ang, J. Kusuma, D.L. Clements, A boundary element method for a second order elliptic partial differential equation with variable coefficients, *Eng. Anal. Bound. Elem.*, Vol.18, No.4, 311-316, 1996.
- [13] D.L. Clements, A boundary integral equation method for the numerical solution of a second order elliptic equation with variable coefficients, *J. Aust. Math. Soc.*, Vol.22(B), 218-228, 1980.
- [14] C. Pozrikidis, Reciprocal identities and integral formulations for diffusive scalar transport and Stokes flow with positiondependent diffusivity or viscosity, *J. Engrg. Math.*, Vol.96, No.1, 595-114, 2016.
- [15] M.A. AL-Jawary, L.C. Wrobel, Radial integration boundary integral and integro-differential equation methods for two-dimensional heat conduction problems with variable coefficients, *Eng. Anal. Bound. Elem.*, Vol.36, No.5, 685-695, 2012.
- [16] O. Chkadua, S.E. Mikhailov, D. Natroshvili, Analysis of direct boundary-domain integral equations for a mixed BVP with variable coefficient, I: equivalence and invertibility, *J. Int. Eqns. Appl.*, Vol.21, No.4, 499-543, 2009.

- [17] D.L. Clements, A fundamental solution for linear second-order elliptic systems with variable coefficients, *J. Engrg. Math.*, Vol.49, No.3, 209-216, 2004.
- [18] D. Colton, R. Kress, *Integral Equation Methods in Scattering Theory*, John Wiley & Sons, Inc., 1983.
- [19] P.W. Partridge, C.A. Brebbia, and L.C. Wrobel, *The Dual Reciprocity Boundary Element Method*, Computational Mechanics Publications, Southampton, 1992.
- [20] D. Colton, R. Kress, *Inverse Acoustic and Electromagnetic Scattering Theory*, Springer-Verlag, Berlin Heidelberg, 1992.
- [21] I. Brunton, Solving variable coefficient partial differential equations using the boundary element method, Ph.D. Thesis, The University of Auckland, Auckland, 1996.